

Copyright  
by  
Nicholas Ryan Delone  
2010

**The Thesis Committee for Nicholas Ryan Delone  
Certifies that this is the approved version of the following thesis:**

**Surface Enhanced Raman Spectroscopy  
of Olivine Type Battery Cathode  $\text{LiFePO}_4$**

**APPROVED BY  
SUPERVISING COMMITTEE:**

**Supervisor:**

---

Keith J. Stevenson

---

David A. Vanden Bout

**Surface Enhanced Raman Spectroscopy  
of Olivine Type Battery Cathode  $\text{LiFePO}_4$**

**by**

**Nicholas Ryan Delone, B.S.**

**Thesis**

Presented to the Faculty of the Graduate School of

The University of Texas at Austin

in Partial Fulfillment

of the Requirements

for the Degree of

**Master of Arts**

**The University of Texas at Austin**

**August 2010**

## **Dedication**

To Tricia and my wonderful family.

## Acknowledgements

I would like to thank Professor Keith Stevenson for the opportunity he has given me to learn and grow under him during graduate school. I appreciated the fact that although he does expect progress and results, he does not micromanage like so many other professors do. I also appreciate that he was willing to go to bat for me and for the financial support that allowed me to focus on my research.

I'd like to thank my fellow Stevenson Group lab members for their support, input and discussion during my time at UT. Special thanks go out to Jaclyn Wiggins-Camacho for showing me the ropes from my first day on campus and showing me work ethic second to none.

I also need to thank my fellow graduate students, Jared Shaw (a fellow Red Raider) and Julia Aponte from the Brodbelt Lab. They were able to help me balance out my graduate student life with play along with the work. I will miss our Austin adventures together from our football games in the sea of burnt orange and the sweltering sun to our Sixth Street outings that some of us do not recall. I'd also like to thank the Brodbelt Lab as a whole, for including me in their many breaks and post-work activities. From going for 'fro yo' on Wednesdays to our outings to Cain and Abel's, there is never a dull moment with them.

## **Abstract**

### **Surface Enhanced Raman Spectroscopy of Olivine Type Battery Cathode $\text{LiFePO}_4$**

Nicholas Ryan Delone, M.A.

The University of Texas at Austin, 2010

Supervisor: Keith J. Stevenson

This thesis explores the use of Raman Spectroscopy to study the battery cathode material  $\text{LiFePO}_4$ . Surface Enhanced Raman Spectroscopy (SERS) was incorporated into the study due to fluorescence that traditionally plagues Raman. By imaging  $\text{LiFePO}_4$  nanoparticles, an understanding can be gained of the complex chemistry taking place when the material is lithiated and delithiated at the nanoscale level and the phase changes of the material that occur during this process. The use of bimetallic (Au/Ag) SERS substrates allowed for more stable substrates with longer shelf life compared single metal Ag substrates. Further tuning of these substrates can be applied to the ever evolving science of energy storage material technology as a way to track phase changes in the material.

## Table of Contents

List of Figures .....	x
List of Tables .....	xii
Chapter 1 Energy Storage Materials.....	1
1.1 Introduction .....	1
Chapter 2 Surface Enhanced Raman Spectroscopy.....	12
2.1 Introduction .....	12
2.2 Experimental.....	13
2.2.1 Initial Raman Experiments .....	13
2.2.2 SERS Substrate Preparation .....	15
2.2.3 UV-Vis Diffuse Reflectance Spectroscopy .....	21
2.2.4 Atomic Force Microscopy.....	21
2.2.5 Scanning Electron Microscopy.....	21
2.2.6 LiFePO <sub>4</sub> Deposition .....	22
2.3 Results and Discussion.....	22
2.3.1 Initial Raman Experiments .....	22
2.3.2 UV-Vis Diffuse Reflectance Spectroscopy .....	25
2.3.3 Atomic Force Microscopy.....	27
2.3.4 Scanning Electron Microscopy.....	27
2.3.5 SERS Substrate Stability .....	31
2.4 Conclusions .....	35
Chapter 3 Electrochemical Cell Design.....	39
3.1 Introduction .....	39
3.2 Experimental.....	41
3.2.1 <i>in situ</i> SERS Electrochemical Cell Design .....	41
3.3 Discussion and Conclusions .....	44

Chapter 4 Isolation of LiFePO <sub>4</sub> Nanoparticles.....	45
4.1 Introduction .....	45
4.2 Experimental .....	46
4.2.1 Single LiFePO <sub>4</sub> Nanoparticle Deposition .....	46
4.3 Results and Discussion.....	46
4.3.1 Scanning Electron Microscopy.....	46
4.3.2 Raman Spectroscopy Studies.....	47
4.4 Conclusions .....	50
Chapter 5 Future Directions .....	52
5.2 Experimental .....	54
5.2.1 Au Nanobowl Preparation .....	55
5.3 Results and Discussion.....	56
5.2.1 Atomic Force Microscopy.....	56
5.3.2 Scanning Electron Microscopy.....	56
5.4 Conclusions .....	61
References .....	62
Vita .....	68



## List of Figures

- Figure 1.1: (a) Schematic of a Li ion battery and (b) a Ragone plot of current energy sources. .... 4
- Figure 1.2: (a) Olivine structure of  $\text{LiFePO}_4$  showing Li in 1D channels. Lithium ions are green, iron octahedral in blue and phosphorus tetrahedral in gold. Reproduced from ref. 11 with permission from the American Chemical Society. (b) Spinel structure of  $\text{LiMn}_2\text{O}_4$ . Mn atoms are yellow, Li atoms are red and O atoms are light blue. Reproduced from ref 10, with permission of the International Union of Crystallography.. (c) Layered oxide structure of  $\text{LiCoO}_2$ .  $\text{CoO}_6$  octahedra are shaded in blue. Lithium ions are shown in beige. Adapted by permission from Macmillan Publishers Ltd from ref 6, copyright 2003..... 7
- Figure 2.1: SEM image of multilayer PS spheres seen along the fracture line of the SERS substrate. .... 17
- Figure 2.2: SEM image of a single monolayer of PS spheres can be seen on the SERS substrate..... 18
- Figure 2.3: Schematic of SERS substrate sample holder ..... 19
- Figure 2.4: Schematic representation of the  $\text{LiFePO}_4$  deposition process onto the SERS substrate..... 23
- Figure 2.5: Unenhanced  $\text{LiFePO}_4$  spectra from initial Raman studies. ... 24
- Figure 2.6: UV-Vis diffuse reflectance spectra shows the location of the plasmon for the 160 nm AgFON SERS substrate. .... 26
- Figure 2.7: UV-Vis Diffuse reflectance showing the red-shift of the plasmon as the metal composition varies. .... 28

Figure 2.8: Atomic force microscope topography image of the ambient atmosphere dried FON substrates as viewed from (a) above and (b) at an angle.....	29
Figure 2.9: Atomic force microscope topography image of the desiccator dried FON substrates as viewed from (a) above and (b) at an angle .....	30
Figure 2.10:SEM image of SERS substrate dried under ambient lab conditions.....	32
Figure 2.11:SEM image of SERS substrate dried under desiccator drying conditions.....	33
Figure 2.12:LiFePO <sub>4</sub> Raman spectra from initial AgFON SERS substrates .....	34
Figure 2.13:Surface enhanced spectra of LiFePO <sub>4</sub> on the bimetallic SERS substrate. ....	36
Figure 2.14:LiFePO <sub>4</sub> comparison spectra of “traditional” Raman vs. SERS experiments.....	37
Figure 3.1: A schematic of the working electrode of the electrochemical cell.....	42
Figure 3.2: (a) Top view and (b) side view of the electrochemical cell ....	43
Figure 4.1: SEM image of the SERS substrate covered with a high concentration of LiFePO <sub>4</sub> nanoparticles.....	48
Figure 4.2: SEM image of LiFePO <sub>4</sub> nanoparticles isolated on the SERS substrate. ....	49
Figure 4.3: SERS spectra of isolated LiFePO <sub>4</sub> nanoparticles .....	51
Figure 5.1: Atomic force microscope image of Au nanobowl, with surface periodicity on right.....	57
Figure 5.2: Atomic force microscope topography image of Au nanobowls at an angle .....	58

Figure 5.3: SEM image of highly ordered Au nanobowls .....	59
Figure 5.4: SEM image of $\text{LiFePO}_4$ nanoparticle deposited in Au nanobowls.....	60

## List of Tables

Table 1.1: Li-ion Battery Cathode Material and Structure Type .....	6
---	---

# Chapter 1

## Energy Storage Materials

### 1.1 INTRODUCTION

Today's growing concern about the environment and renewable energy sources for powering automobiles, portable electronic devices and even buildings and houses has led to exciting emerging research in science.<sup>1</sup> It is now clear that emissions from automobiles, energy production (electricity from coal burning), industrial factories, etc. have had a negative effect on the climate and have played a role in what many scientists have recognized as climate change.<sup>2</sup> Currently, society is trying to go 'green.' This includes using recyclable shopping bags instead of traditional paper or plastic bags and finding methods of transportation that don't include vehicles that get very poor gas mileage and have high emissions. Ten years ago, many people drove large SUV's and large trucks, but that trend has changed as the attitude of drivers have evolved. For automobile manufacturers, this has led to a strong push for research and development for hybrid electric vehicles (HEVs), which run on both gasoline engines and also off of batteries<sup>3</sup> and fully electric vehicles (EVs), which run solely off of batteries. Energy density is defined as the amount of energy, in Watt-hours (Wh) a material can store per kilogram (kg). Power density is the measure of power in Watts (W) per kilogram (kg) of a material. Both can be represented in a single graph called a Ragone plot for different energy storage devices. A representative Ragone plot of current energy sources, adapted from

reference 4 is shown in Figure 1.1. Fuel cells have high energy density, but low power density. In contrast, capacitors have high power density, but low energy density. To solve the energy demand problem, the scientific community is diligently researching alternative, renewable methods to power the world, such as solar power, geothermal power and wind power. When designing materials to power automobiles, electronics and other such devices, the components which make up the materials must be plentiful, inexpensive, nontoxic and environmentally benign.

This study focuses on batteries, which are efficient storage devices that generally have output energy (Wh/kg) greater than 90% of input energy.<sup>4</sup> In order to produce commercially viable fully EVs for consumers, battery technology needs to improve to match both the energy and power density of internal combustion engines. The introduction of lithium ion battery technology by Sony in 1991 has played a key role in the portable electronic revolution. Lithium ion batteries have high volumetric and gravimetric energy densities which leads to small, lightweight batteries.<sup>5</sup> This is important when discussing vehicle applications, because weight is of particular concern when designing vehicles. Batteries are an important part of everyday life for many reasons. They power our laptops, iPod's, MP3 players, cell phones and help start and power our vehicles. Lithium ion (Li ion) batteries are currently one of the most used rechargeable battery by consumers. Other rechargeable batteries include lead-acid batteries, which are used in automobiles, nickel-cadmium and nickel-metal

hydride. Batteries are composed of a cathode, anode and electrolyte. A schematic of a Li ion battery is shown in Figure 1.1. The most common anode material used in commercial batteries is graphitic carbon. The electrolyte used in commercial Li ion batteries is Lithium Hexafluorophosphate ( $\text{LiPF}_6$ ). The cathode is composed of a metal oxide that is mixed with carbon to increase the electron conductivity, and a polymer binder to stabilize and support the cathode material. The cathode, along with the electrolyte is what limits the capacity, or amount of available charge per hour of the battery. Since this is the limiting factor in battery development, understanding the processes will allow for the designing of better batteries.

The batteries introduced by Sony in 1991 used the layered lithium cobalt oxide ( $\text{LiCoO}_2$ ), which is the most commonly used cathode<sup>6</sup> material rechargeable batteries, and has a potential of 4 V vs.  $\text{Li}^+/\text{Li}$ .<sup>7</sup> Although it has good potential (high voltage) vs.  $\text{Li}^+/\text{Li}$  reference electrode, it also presents safety concerns when deeply charged and it contains toxic cobalt. Large volume expansion is a problem that plagues  $\text{LiCoO}_2$  and only allows for the use of approximately 50% of the capacity.<sup>8</sup>  $\text{LiCoO}_2$  is a layered oxide material in which the cobalt and oxygen is one layer and the lithium is another layer. When  $\text{LiCoO}_2$  is deeply charged, it undergoes a large volume expansion following the removal of Li due to electrostatic repulsion between the  $\text{CoO}_2$  layers.<sup>9</sup> The deintercalation

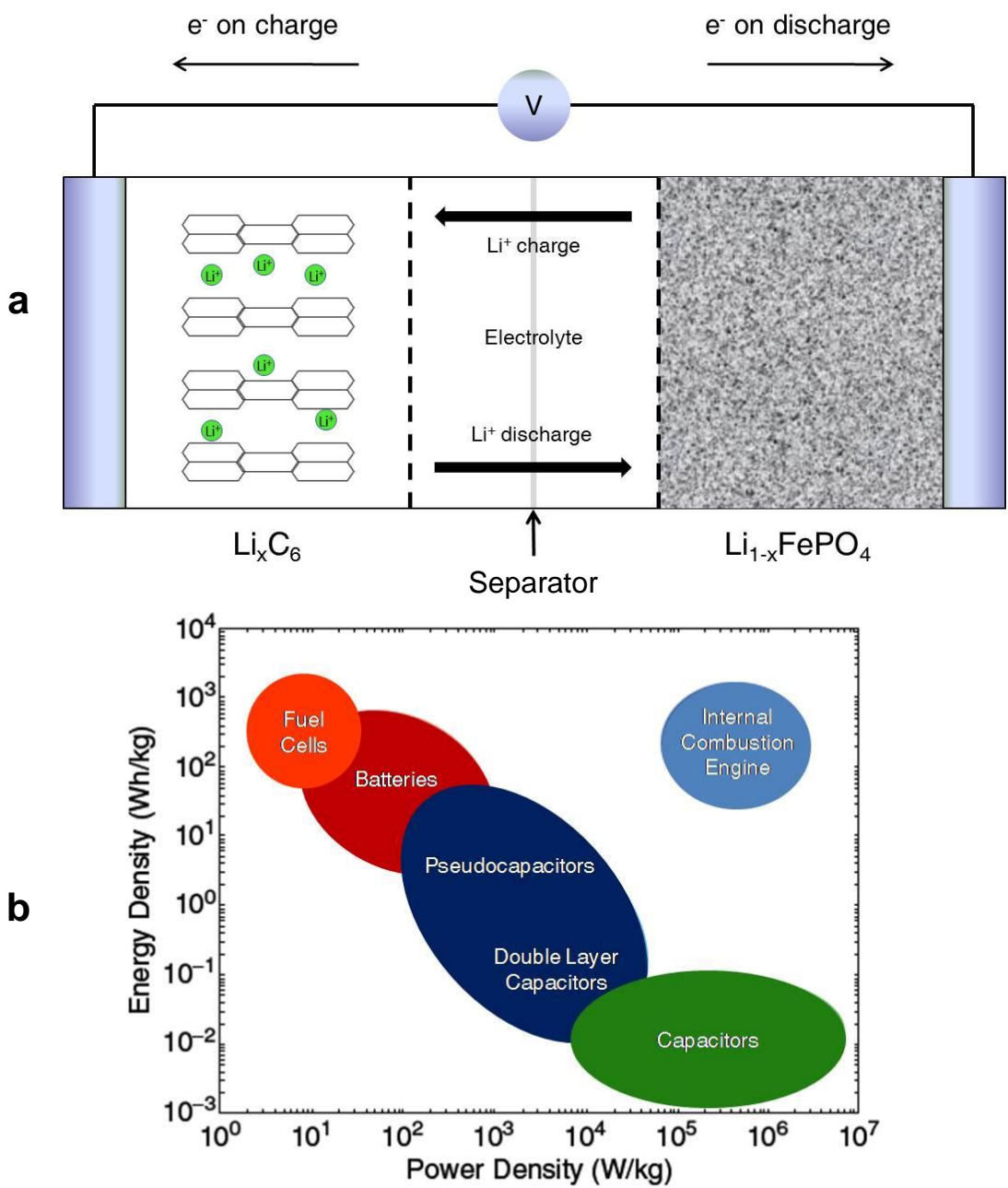


**Figure 1.1** (a) Schematic of a Li-ion battery, adapted from ref. 1 and (b) a Ragone plot of current energy sources, adapted from ref. 4.



of lithium out of the oxide layers causes the breaking of the Co—O bonds which causes the evolution of oxygen gas. The evolution of oxygen along with the overheating the highly flammable organic electrolyte can lead to swelling of the battery, which can then explode and the organic electrolyte can catch fire. This has been a problem in laptop batteries in the past which have since been improved to include a safety feature that prevents the overcharging of the battery. Materials used for rechargeable Li ion batteries are layered oxides<sup>6</sup>, spinel<sup>10</sup>, olivines<sup>11</sup> and composite materials. Figure 1.2 illustrates the structural differences between layered oxides, spinel and olivine materials.

There is currently a fundamental lack of understanding of how thermodynamic properties of such materials change when they go from bulk to nanoscale.<sup>4</sup> With respect to  $\text{LiFePO}_4$ , there are outstanding questions that need to be answered. There are complex interfaces at the surface and within the nanoparticle and there is a need to study these to elicit information that could lead to an explanation of what chemical processes are taking place on the nanoscale level. The benefit of moving to smaller and smaller nanoparticles is the increasing of the surface area and decreasing the diffusion length for the Li ions and the accompanying electrons. Shorter diffusion lengths in this material could lead to increased charge/discharge rates and could also demonstrate the one phase reaction.<sup>12, 13</sup> Equation 1.1 shows the proposed two phase reaction of a  $\text{LiFePO}_4$  nanoparticle.<sup>14</sup>

**Table 1.1 Li-ion Battery Cathode Material and Structure Type**

<b>Battery Material</b>	<b>Structure Type</b>
LiCoO <sub>2</sub>	Layered-Oxide
LiMn <sub>2</sub> O <sub>4</sub>	Spinel
LiFePO <sub>4</sub>	Olivine

As previously mentioned, batteries are composed of two electrodes (anode and cathode) and an electrolyte. The electrolyte must have a large potential window, good electron and Li ion conductivity and it must maintain chemical stability with the electrodes within normal and extreme operating temperatures.<sup>15</sup> Electrolytes that have been studied for use in Li ion batteries include polymers, inorganic liquids, ionic liquids, inorganic solids, liquid organic and combinations of electrolytes (i.e. Ionic Liquid + Polymer). The ideal electrolyte for usage in batteries would be non-flammable, low cost and low to non-toxic.<sup>15</sup>

The battery with LiFePO<sub>4</sub> as the cathode and graphitic carbon as the anode works by shuttling and intercalating Li ions between the anode and cathode and passing the electrons via an external circuit as shown in Figure 1.1. The electrolyte assists the Li ion transfer from the cathode to anode on charging and discharging. Upon charging, the electrons leave the cathode and are passed through the positive current collector. From here, the electrons are passed

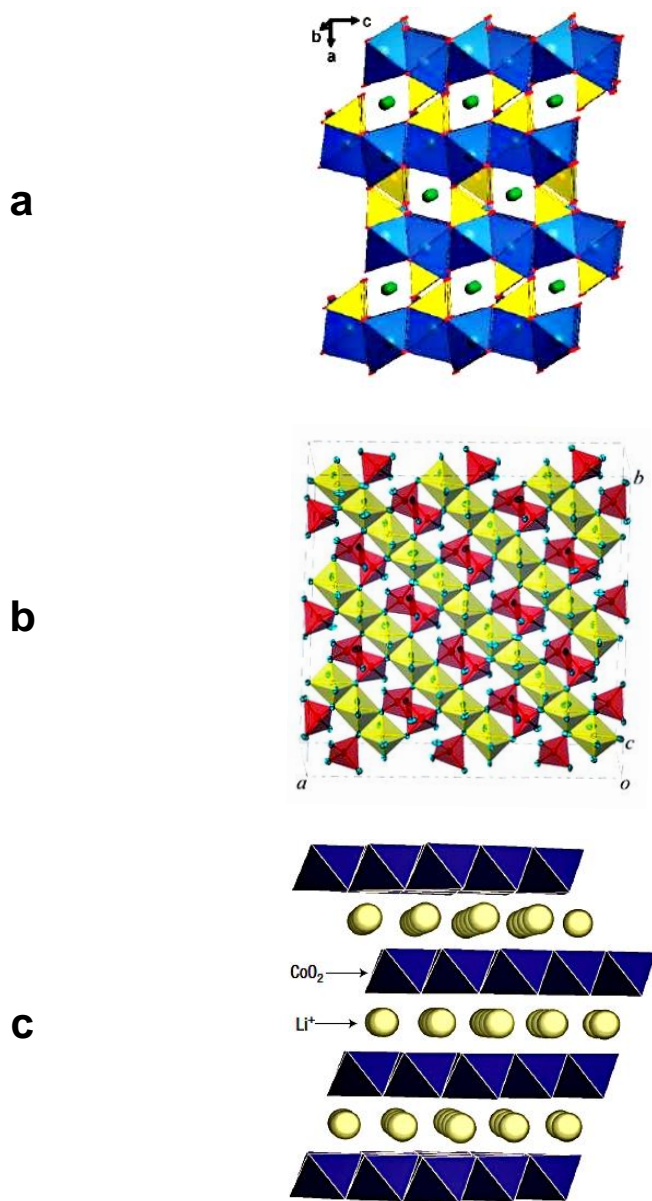


**Figure 1.2** (a) Olivine structure of  $\text{LiFePO}_4$  showing Li in 1D channels. Lithium ions are green, iron octahedral in blue and phosphorus tetrahedral in gold. Reproduced from ref. 11 with permission from the American Chemical Society. (b) Spinel structure of  $\text{LiMn}_2\text{O}_4$ . Mn atoms are yellow, Li atoms are red and O atoms are light blue. Reproduced from ref 10, with permission of the International Union of Crystallography. (c) Layered oxide structure of  $\text{LiCoO}_2$ .  $\text{CoO}_6$  octahedra are shaded in blue. Lithium ions are shown in beige. Adapted by permission from Macmillan Publishers Ltd from ref 6, copyright 2003.

through the external circuit on their way to be reunited with the Li ion in the anode. When discharging the battery, the electrons reverse course and flow back to the cathode as the Li ion leaves the graphitic carbon is transported back to the cathode to be reintercalated.

Equation 1.1 – Electrochemical Process of LiFePO<sub>4</sub>



The process of lithiating and delithiating the LiFePO<sub>4</sub> cathode leads to a volume change of approximately 6.5%<sup>14, 16</sup>, with the material shrinking and expanding with the removal and insertion of Li ions, respectively. The P—O bonds lengthen to accommodate Li ions and Fe—O bonds also readjust as Fe goes between the Fe<sup>2+/3+</sup> oxidation states. The olivine structure of LiFePO<sub>4</sub> resists excessive volume change during the charge/discharge process that plagues LiCoO<sub>2</sub>, which has a volume change of approximately 10%, which leads to structural instability of the cathode.<sup>9</sup> The results of these charge/discharge studies show that the smaller volume change of LiFePO<sub>4</sub> is promising for use as a cathode material in Li ion batteries.

One of the unique properties of Li ion batteries is the formation of a solid electrolyte interface (SEI) layer, which controls many properties of the Li ion battery. A SEI layer can be defined as “the layer formed instantaneously upon contact of the metal with the solution and consists of insoluble and soluble reduction products of electrolyte components.”<sup>17</sup> Peled and coworkers<sup>18, 19</sup> have

explained that the SEI performs the task of controlling lithium diffusion, safety, battery shelf life, and cycle life. The formation of the SEI layer on the graphite anode leads to an irreversible capacity loss due to the permanent consumption of lithium ions. Formation of the SEI layer prevents the deposition of metallic dendrites which cause the battery fail due to short circuiting.

Numerous techniques such as X-Ray Diffraction<sup>7, 14, 20-24</sup>, Mössbauer Spectroscopy<sup>21</sup>, FTIR<sup>7, 25, 26</sup>, Raman Spectroscopy<sup>7, 20, 23, 25, 26</sup>, electrochemical<sup>14, 20-24</sup> have been performed on LiFePO<sub>4</sub>. Raman Spectroscopy is a particularly powerful analytical tool that can probe molecular bonds of a material and is surface sensitive. Within the olivine structure of LiFePO<sub>4</sub>, the molecular vibrations of the phosphate groups are predicted to be sensitive to the presence of lithium, as the lithium ions are coordinated to the oxygen atoms which are complexed to the phosphorus atoms.<sup>26</sup> LiFePO<sub>4</sub> has been prepared by various methods such as hydrothermal and solvothermal reactions, sol-gel method<sup>27</sup> and pyrolysis process.<sup>28</sup>

It is the intention of this thesis to further study the complex chemistry that takes place in the cathode material LiFePO<sub>4</sub>. To accomplish this task, Raman Spectroscopy will be employed to study the molecular vibrations of the bonds in phospho-olivine materials. The LiFePO<sub>4</sub> used in this study has been prepared following the microwave solvothermal procedure as described in Murugan et al.<sup>29</sup> Since LiFePO<sub>4</sub> nanoparticles can be made in various dimensions<sup>22, 23</sup>, we are able to study the effects of nanoparticle size vs. charge/discharge kinetics and

phase transition when charging/discharging. Ex-situ Raman studies have shown that the most intense stretching bands observed in  $\text{LiFePO}_4$  are assigned to the  $\nu_1$  and  $\nu_3$  symmetric and anti-symmetric stretching of the  $\text{PO}_4^{3-}$  bonds, respectively.<sup>26, 30</sup> The most intense stretching band ( $\nu_1$ ), is observed at  $\sim 950 \text{ cm}^{-1}$ , with the less intense bands ( $\nu_3$ ) located at  $\sim 1000 \text{ cm}^{-1}$  and  $\sim 1070 \text{ cm}^{-1}$ . These intense bands shift and disappear as  $\text{LiFePO}_4$  is delithiated and changes phase to  $\text{FePO}_4$ . The shifting of these bands can be attributed the olivine structure relaxing as the lithium ions leave the cathode and travel to the anode via the electrolyte.

This thesis is organized into five chapters, with Chapter 1 providing a general introduction and motivation behind the evolution of energy storage materials that concludes with specific discussion on the scope and focus of the research being presented. Chapter 2 describes the use of Raman Spectroscopy to study anode and cathode battery materials and the information that can be obtained, including bond type, bond strength and bond length. Raman Spectroscopy is the ideal technique to study the battery cathode material  $\text{LiFePO}_4$ , because it can study the metal-ligand bonds that make up the olivine structure that are not easily studied by Infrared Spectroscopy. Surface Enhanced Raman Spectroscopy (SERS) is introduced and is used to study the  $\text{LiFePO}_4$ , as a method to eliminate fluorescence signal that traditionally plagues Raman Spectroscopy. The evaluation and tuning of the film over nanosphere (FON) SERS substrates is covered as well. Characterization is critical to producing

substrates that takes into account the excitation source and will provide for the greatest signal enhancement. The analytical tools used are AFM, SEM and UV-Vis reflectance.

Chapter 3 describes the electrochemical cell design for the incorporation of the SERS substrates for  $\text{LiFePO}_4$  in situ Raman studies. In-situ SERS is an ideal technique for the study of single  $\text{LiFePO}_4$  nanoparticles, given the surface enhancement provided by the SERS substrate.

Chapter 4 describes the use of SERS to study isolated  $\text{LiFePO}_4$  nanoparticles. Previous Raman studies on  $\text{LiFePO}_4$  have been done on bulk electrodes, but single nanoparticle SERS analysis has not been done before. Since a single nanoparticle will inherently have a lower signal than a bulk electrode, SERS is an ideal analytical tool to investigate  $\text{LiFePO}_4$  nanoparticles.

Future direction for this research is discussed in Chapter 5. It details the fabrication and characterization of nanobowl SERS substrates and how they can be further tuned and optimized for single  $\text{LiFePO}_4$  nanoparticle detection. These alternative SERS substrates have a unique geometry that can be used to isolate single nanoparticles. The rims of these nanobowls have been shown to generate increased electromagnetic (EM) enhancement that can lead to greater surface enhancement.

## Chapter 2

### Surface Enhanced Raman Spectroscopy

#### 2.1 INTRODUCTION

The use of Raman Spectroscopy for battery materials, both anode and cathode, has been instrumental in understanding the structural, surface and local properties of the material.<sup>31</sup> More specifically, Raman is used to probe the vibrational bonds of the constituent elements that make up the energy storage material. With the help of mathematical models, bond type, bond strength and bond length can all be determined from Raman Spectroscopy. In Popović et al., the authors established a correlation between the Raman stretching wavenumbers of P—O bonds and their bond lengths in inorganic crystalline phosphates.<sup>32</sup> In cathode materials such as  $\text{LiFePO}_4$ , it is of particular interest to study the metal-ligand bonds that aren't as easily studied with Infrared Spectroscopy.<sup>33</sup> Burba et al. showed that ex-situ Raman can be used to study  $\text{LiFePO}_4$  in different states of lithiation<sup>26</sup> by removing the lithium chemically. In their study, the  $\text{LiFePO}_4$  was reacted with various amounts of liquid  $\text{Br}_2$  in acetonitrile to achieve different stoichiometric values of lithium content. The  $\text{Li}_{1-x}\text{FePO}_4$  was then washed, dried and analyzed via Raman. While this study was helpful in studying the changes that  $\text{LiFePO}_4$  undergoes as lithium is removed, it did so by a process that is not present in actual batteries. Electrochemical delithiation is a much more relevant way to study these electrode materials.



## 2.2 EXPERIMENTAL

### 2.2.1 Initial Raman Experiments

The  $\text{LiFePO}_4$  used in this study was prepared following the microwave-solvothermal (MW-ST) method as described in Murugan et al.<sup>29</sup> Initial Raman experiments were performed by taking neat  $\text{LiFePO}_4$  and depositing a small quantity of the material on a microscope slide, adding a drop of ethanol to the slide to secure the material, then evaporating off the excess ethanol. The slide was then mounted under the microscope objective of a Renishaw inVia Raman Microscope. The excitation source used is a 50 mW, 514.5 nm Argon ion laser. The power output was reduced to 5 mW out of concern for irreversible damage to the exposed area of the sample. The samples were typically exposed for 60 seconds and two accumulations were taken. It is important to note that while Raman Spectroscopy is a powerful analytical tool, it is prone to signal interference such as fluorescence. Multiple wavelengths (422 nm, 755 nm) were investigated, however the observed fluorescence cannot be eliminated in this manner. In the microwave-solvothermal  $\text{LiFePO}_4$  preparation method reported by Murugan<sup>29</sup>, the  $\text{LiFePO}_4$  samples are thoroughly washed of all precursor chemicals after synthesis with acetone, so precursor chemicals can be eliminated as the cause of fluorescence. It was determined that the most likely reason for fluorescence of the sample is the fact that the material is a whitish-grey color after synthesis and washing.

An alternative method of utilizing Raman to study these  $\text{LiFePO}_4$  nanoparticles was employed to improve the spectra. Surface Enhanced Raman Spectroscopy (SERS) is a process in which analytes (molecules or nanoparticles) are adsorbed onto an enhancing surface, which is typically a metal, and generates an increase in the Raman scattering signal from the  $10^2 - 10^{15}$  range.<sup>34-36</sup> These large enhancements correspond to single molecule SERS detection. To fully understand the concept of SERS, the topic of Localized Surface Plasmon Resonance (LSPR) needs to be introduced. Plasmon can be defined as the coherent oscillation of the surface conduction excited by electromagnetic (EM) radiation from the excitation source. The EM field enhancement of SERS is attributed to LSPR.<sup>37</sup> When the excitation source (laser) interacts with the surface of the metal, it accelerates the movement of the conduction electrons into a wavelike motion. This motion increases the electron cloud distortion of the molecule or nanoparticle, which leads to large increases in the emitted radiation from the molecules and nanoparticles. The larger or more intense the emitted radiation, the stronger the Raman signal will be. One of the most widely analyzed single molecule system is Rhodamine 6G (R6G).<sup>35, 38-40</sup> The SERS enhancement of these single molecules takes place by depositing a solution of R6G ( $\mu\text{M} - \text{pM}$ ) onto gold or silver nanoparticles, nanoparticle films, film over nanosphere (FON) or other lithography prepared substrates.

### 2.2.2 SERS Substrate Preparation

The SERS substrates that were used in this study are adapted from the method described by Van Duyne.<sup>41, 42</sup> The SERS substrates were prepared by first cleaning microscope cover slips (25 mm dia.) first in a Piranha bath (3:1 H<sub>2</sub>SO<sub>4</sub>/30% H<sub>2</sub>O<sub>2</sub>) followed by rinsing with 18 mΩ nanopure water until neutral pH followed by immersion in a base bath (5:1:1 H<sub>2</sub>O/H<sub>2</sub>O<sub>2</sub>/NH<sub>4</sub>OH) also followed by rinsing with 18 mΩ nanopure until neutral pH is attained. The cover slips are then stored in a sealed beaker that contains 18 mΩ nanopure water. Four cover slips are removed from the storage beaker and then placed into a petri dish that has been divided into four sections. A drop of 18 mΩ nanopure water is added to each cover slip and then 5 μL of 4% 320 nm polystyrene (PS) sphere/sulfate solution (Microgenics Corp.) is added to each cover slip and hand swirled for 60 seconds, and dried in a desiccator for 12 hours.

When the substrates were initially being prepared with 20 μL of PS nanospheres, the AFM images showed mostly uniform, periodic surfaces. When the same samples were analyzed via SEM, it was revealed that there was a multilayer of PS spheres and not the monolayer that was expected. This feature of the substrate was detected at the surface fracture regions and up to two additional layers could be counted. In light of these results, adjustments were made to the substrate preparation process. The volume of nanospheres added to the cover slips was reduced to 10 μL, which still yielded a multilayer surface as detected by SEM. The volume of PS used was further reduced to 5 μL and was

confirmed by SEM as finally achieving a monolayer on the surface of the cover slip. Figures 2.1 and 2.2 show the progression from multilayer PS spheres to monolayer spheres on the cover slip.

After drying, the cover slips are then placed (with nanospheres facing down) into a custom made aluminum sample holder for use in a thermal deposition chamber. A schematic of the sample holder is shown in Figure 2.3. Metal deposition was carried out in a Denton Thermal Evaporation Chamber. The metal Ag pellets (Kurt J. Lesker, 99.99% pure) or Au wire (Hauser & Miller Co., 99.95% pure), is placed in a tungsten sample boat and mounted to electrical contacts inside the chamber. The sample holder was mounted to a rotation apparatus inside the chamber and then the chamber is pumped down to  $\sim 10^{-5}$  torr. Rotation of the sample holder was used to ensure a uniform coating of metal. Once the chamber reached the proper pressure, current was applied to the tungsten boat containing the target metal. The current was increased slowly until the Quartz Crystal Microbalance (QCM) registered that the metal was vaporized and was being deposited. There is a shutter inside the chamber that covers the sample holder in order to protect it from organic impurity burnoff during the initial heating of the tungsten sample boat. It is removed and then the metal is deposited on the surface of the hexagonal close packed (HCP) nanospheres.

For the 320 nm nanospheres, UV-Vis reflectance helped determine that 160 nm of Ag was needed to produce the plasmon in the proper location, relative to the excitation source, for the excitation source and the emission wavelengths

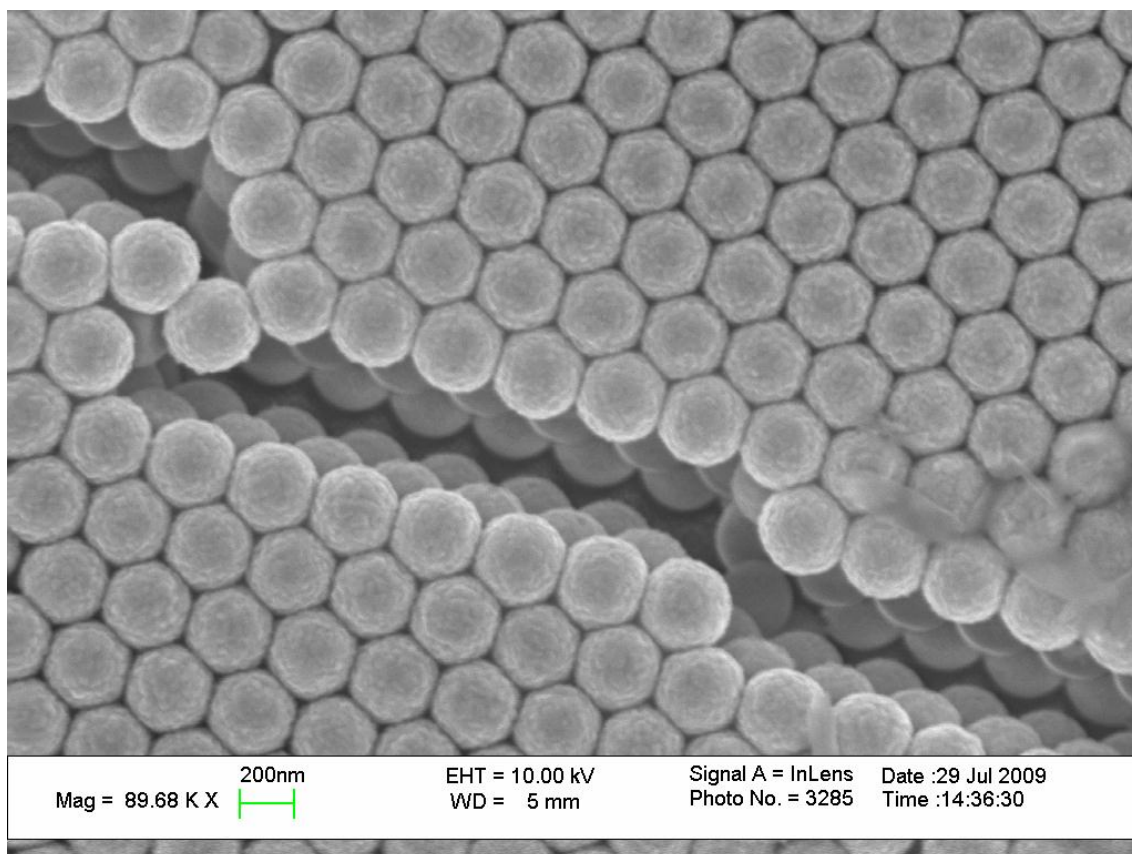


**Figure 2.1** SEM image of multilayer PS spheres seen along the fracture line of the SERS substrate.

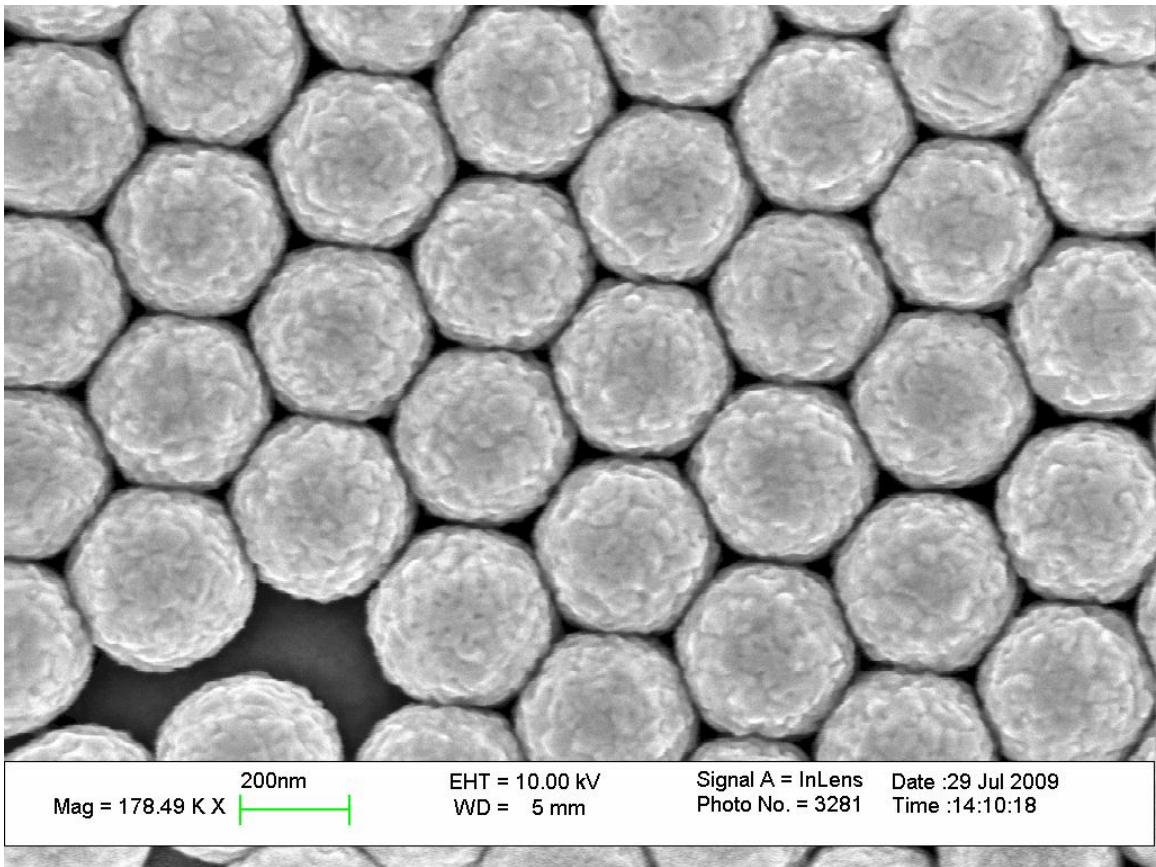


**Figure 2.2** SEM image of a single monolayer of PS spheres can be seen on the SERS substrate.

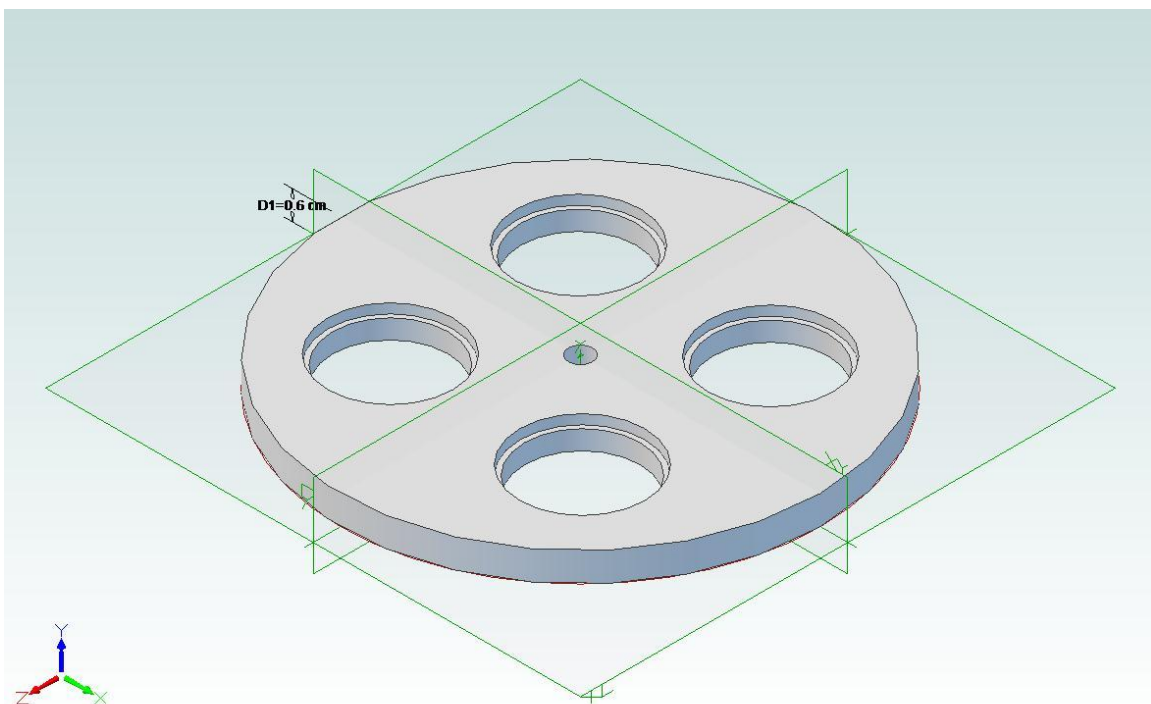


**Figure 2.3** Schematic of SERS substrate sample holder.

of the  $\text{LiFePO}_4$  nanoparticle. To be specific, the location of the plasmon should lie to the red shifted relative to the excitation source and blue shifted relative to the emission wavelength of the  $\text{LiFePO}_4$ . After the desired thickness (160 nm) is attained, the shutter automatically covers the sample holder to prevent excess metal deposition. The applied current is slowly decreased to zero and the power to the contacts is turned off. The chamber is finally returned to atmospheric pressure and the newly created SERS substrates can be removed and stored in a desiccator for use at a later time.

For SERS substrates, it is important that they are uniform, reproducible and easily tunable. There are several analytical tools that are employed to confirm these traits for the SERS substrates used in this study. At first, the substrates were allowed to dry under ambient conditions in the lab and after different optimization procedure the substrates were dried in a desiccator.

Atomic Force Microscopy (AFM) was used to analyze and image the substrates after they had dried. The first use of AFM to analyze a 3D SERS substrate was reported by Van Duyne<sup>43</sup> and associates. The authors demonstrated that AFM could be used to accurately measure the surface roughness and thickness of the deposited metal. They then compared this information with the recorded enhancement factor of their substrates to see how well it corresponded with EM theory. This work laid the groundwork for the use of AFM to characterize the SERS substrates used in this study.



### **2.2.3 UV-Vis Diffuse Reflectance Spectroscopy**

To determine the location of the surface plasmon, UV-Visible Spectroscopy (Cary 5000 UV-Vis-NIR) in the diffuse reflectance set-up was used. The SERS substrates that were dried under ambient conditions showed disorder that was visible via AFM and SEM. Since the surfaces were mostly uniform, it was assumed that if the substrates were prepared and dried in the same fashion, they should have the same plasmon peak location. After scanning the 200-800 nm range in the reflectance set-up, the location of the plasmon on the substrates coated with 160 nm Ag was  $518.5 \pm 7.5$  nm for four substrates prepared at the same time with the same method. This standard deviation is unacceptable in regards to SERS substrates preparation, since plasmon location must be known to achieve the greatest enhancement.

### **2.2.4 Atomic Force Microscopy**

The Digital Instruments Bioscope AFM was used in Tapping Mode™ and silicon tips were used (Budget Sensors Tap300Al-G, 300 kHz, 40 N/m). Samples were mounted on regular glass microscope slide and the slide was put under vacuum suction to prevent the sample from moving. Different sections of the FON substrates were chosen and analyzed to give a good representation of the substrate as a whole.

### **2.2.5 Scanning Electron Microscopy**

Along with the need to regulate sphere packing to tune the metal plasmon location, the plasmon can also be tuned with the thickness and type of metal

deposited. As discussed previously, the initial substrates were prepared with 160 nm of Ag which yielded a plasmon located at 518 nm. The effect of metal type and thickness on the location of the plasmon was also studied during the SERS fabrication process. The bimetallic substrates studied were composed of an Ag base layer and an Au top layer (Ag/Au). SEM is another analytical tool that can be used to study and characterize these samples since they contain Ag and/or Au.

### **2.2.6 LiFePO<sub>4</sub> Deposition**

In order to use LiFePO<sub>4</sub> on the SERS substrate, it needs to be deposited on the surface in a small enough layer in which it can utilize the metal surface to enhance the Raman signal. To do this, neat LiFePO<sub>4</sub> powder is prepared and diluted to  $\sim 10^{-3}$  M in ethanol. The solution is then drop-cast onto the SERS substrates and dried in a vacuum oven to evaporate the ethanol, leaving a light coating of the whitish-grey nanoparticles on the surface. The samples were then analyzed via Raman. A schematic representation of LiFePO<sub>4</sub> deposition is shown in Figure 2.4.

## **2.3 RESULTS AND DISCUSSION**

### **2.3.1 Initial Raman Experiments**

Results from the initial “traditional” Raman studies showed that only the symmetric stretching band of PO<sub>4</sub><sup>3-</sup> at 950 nm was weakly observed above the baseline. Spectra from this experiment can be seen in Figure 2.5.

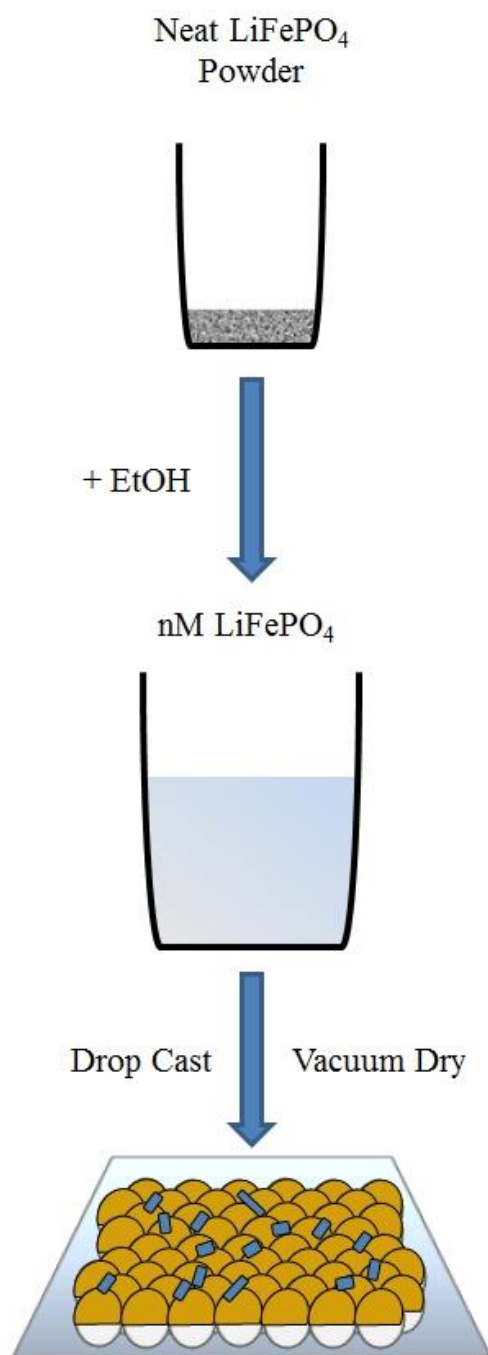


**Figure 2.4** Schematic representation of the LiFePO<sub>4</sub> deposition process onto the SERS substrate.

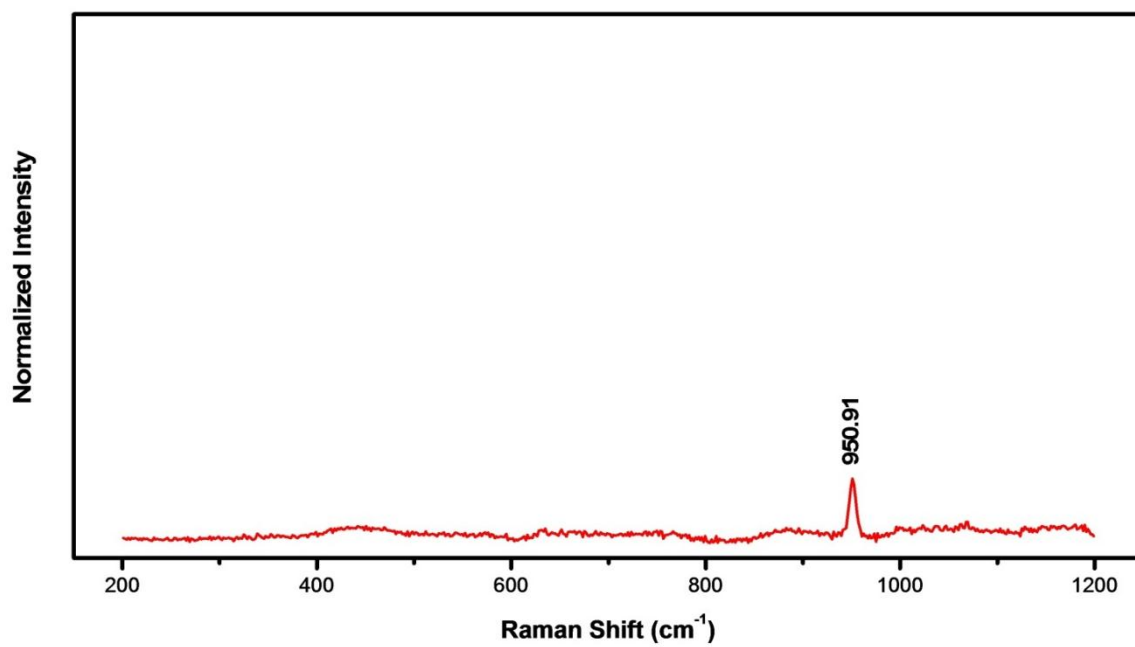


**Figure 2.5** Unenhanced LiFePO<sub>4</sub> spectra from initial Raman studies.

The anti-symmetric stretching  $\text{PO}_4^{3-}$  bands should have been observed at  $1000\text{ cm}^{-1}$  and  $1070\text{ cm}^{-1}$  as well. Even after changing excitation sources to blue (442 nm) and red (785 nm), only the band at 950 nm was observed, corresponding to the symmetric  $\text{PO}_4^{3-}$  stretch.

### **2.3.2 UV-Vis Diffuse Reflectance Spectroscopy**

Even though four SERS substrates were made at once using the same method, it was unknown as to why they yielded varying plasmon peak locations. It was determined that the varying atmospheric conditions in the lab were the cause of the surface fractures and varying surface plasmon peak locations. To improve HCP, the atmospheric conditions needed to be controlled. Drying the substrates in a desiccator was the chosen method, in order to maintain a constant humidity. To test whether the desiccator could improve sphere packing and narrow the plasmon standard deviation, substrates were again prepared and dried in a desiccator. The SERS substrates were subsequently characterized with AFM, SEM and UV-Vis. Results from the desiccator dried substrates were much improved from ambient lab drying. UV-Vis reflectance showed that the plasmon was located at  $518.5 \pm 0.5\text{ nm}$  for the four substrates, which shows a much tighter and reasonable standard deviation. Figure 2.6 shows the plasmon location of the 160 nm AgFON SERS substrate.

Three different metallic compositions, each adding up to 160 nm were studied: 140/20 nm, 120/40 nm and 100/60 nm of Ag to Au ratio. UV-Vis

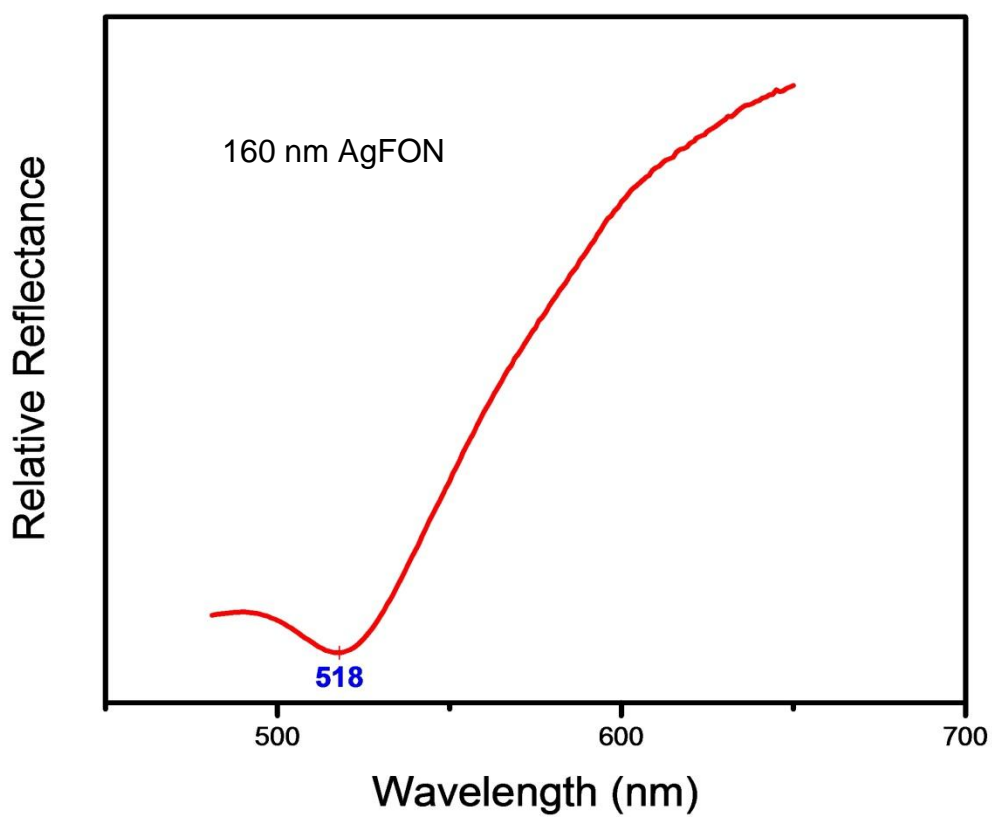


**Figure 2.6** UV-Vis diffuse reflectance spectra shows the location of the plasmon for the 160 nm AgFON SERS substrate.

reflectance spectra showed that the plasmon of the 140/20 nm substrate was located at 537 nm, the plasmon of the 120/40 nm was located at 561 nm and the plasmon of the 100/60 nm substrate was located at 605 nm. Figure 2.7 shows the red shift as metal composition varies. Due to the excitation wavelength being 514.5 nm and the LiFePO<sub>4</sub> emission wavelengths starting at 540 nm, the 140/20 nm substrate was chosen to carry out the LiFePO<sub>4</sub>-SERS study.

### **2.3.3 Atomic Force Microscopy**

AFM results of the ambient dried FON substrates showed that there was some HCP sphere packing, but it also showed surface dislocations. In Figure 2.8, the HCP spheres as well as the surface fractures can be seen. When the FON substrates were dried in the controlled atmosphere of the desiccator, the AFM results showed that the sphere packing was much improved and showed only minor surface dislocations. Figure 2.9 shows the highly uniform HCP FON substrates.

### **2.3.4 Scanning Electron Microscopy**

The results of the SEM study of the different substrate drying methods confirm the AFM results. SEM confirmed that the surface of the substrate dried in ambient conditions was mostly HCP and an expanded imaging window showed the surface fractures to be much longer and more prevalent. Investigation of the desiccator drying method with SEM showed greatly improved sphere packing (HCP) and also showed a small degree of square packing. The substrates that were dried in the ambient atmosphere, where the humidity varies on a daily basis

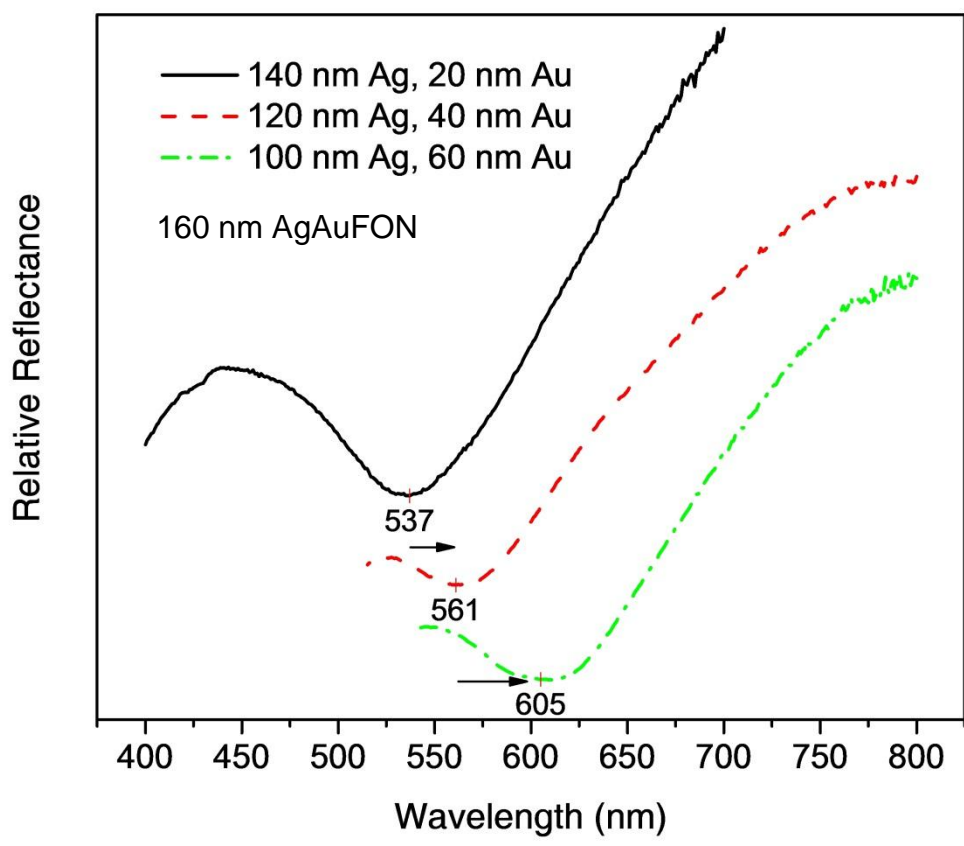


**Figure 2.7** UV-Vis Diffuse reflectance showing the red-shift of the plasmon as the metal composition varies.



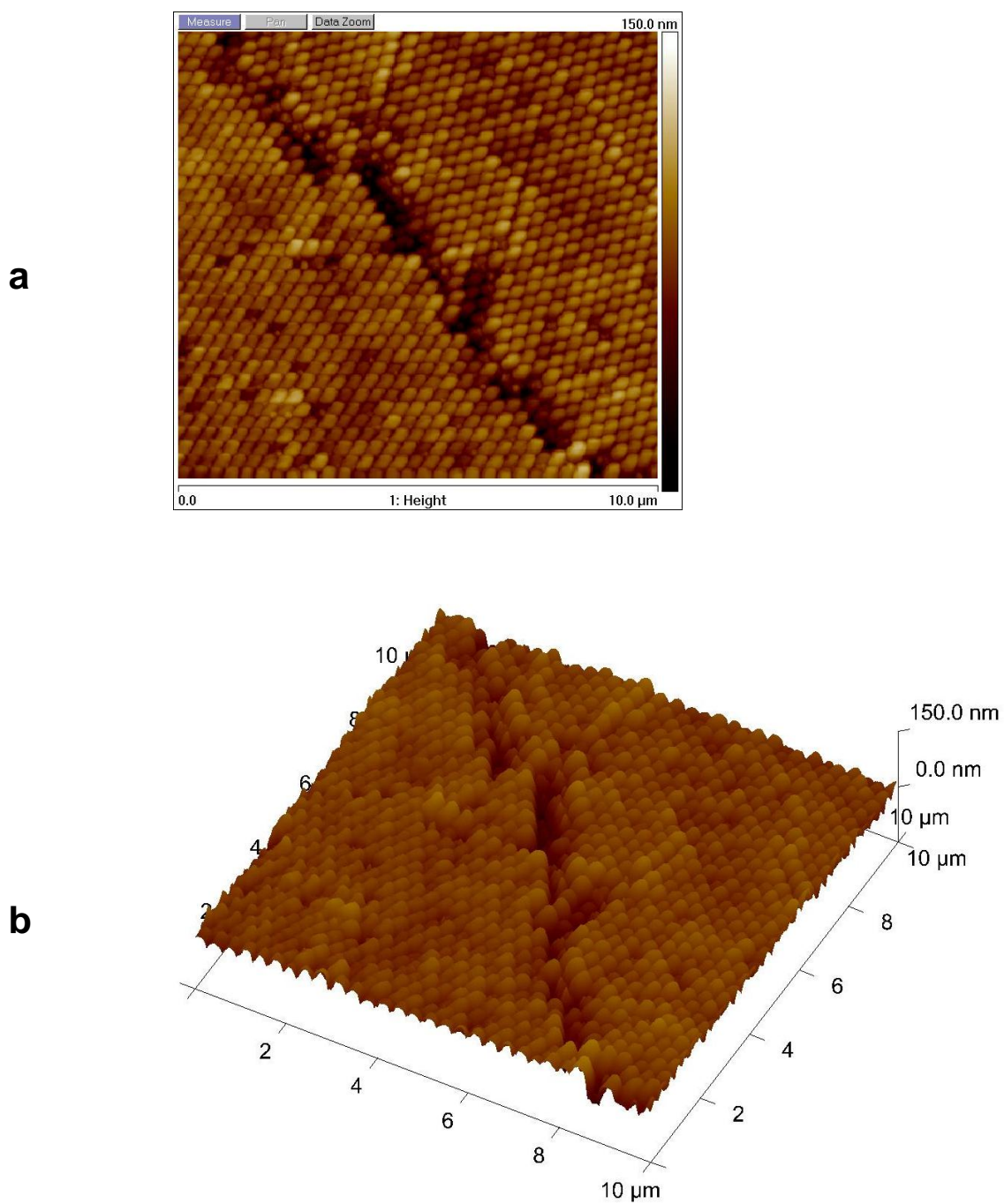


**Figure 2.8** Atomic force microscope topography image of the ambient atmosphere dried FON substrates as viewed from (a) above and (b) at an angle.

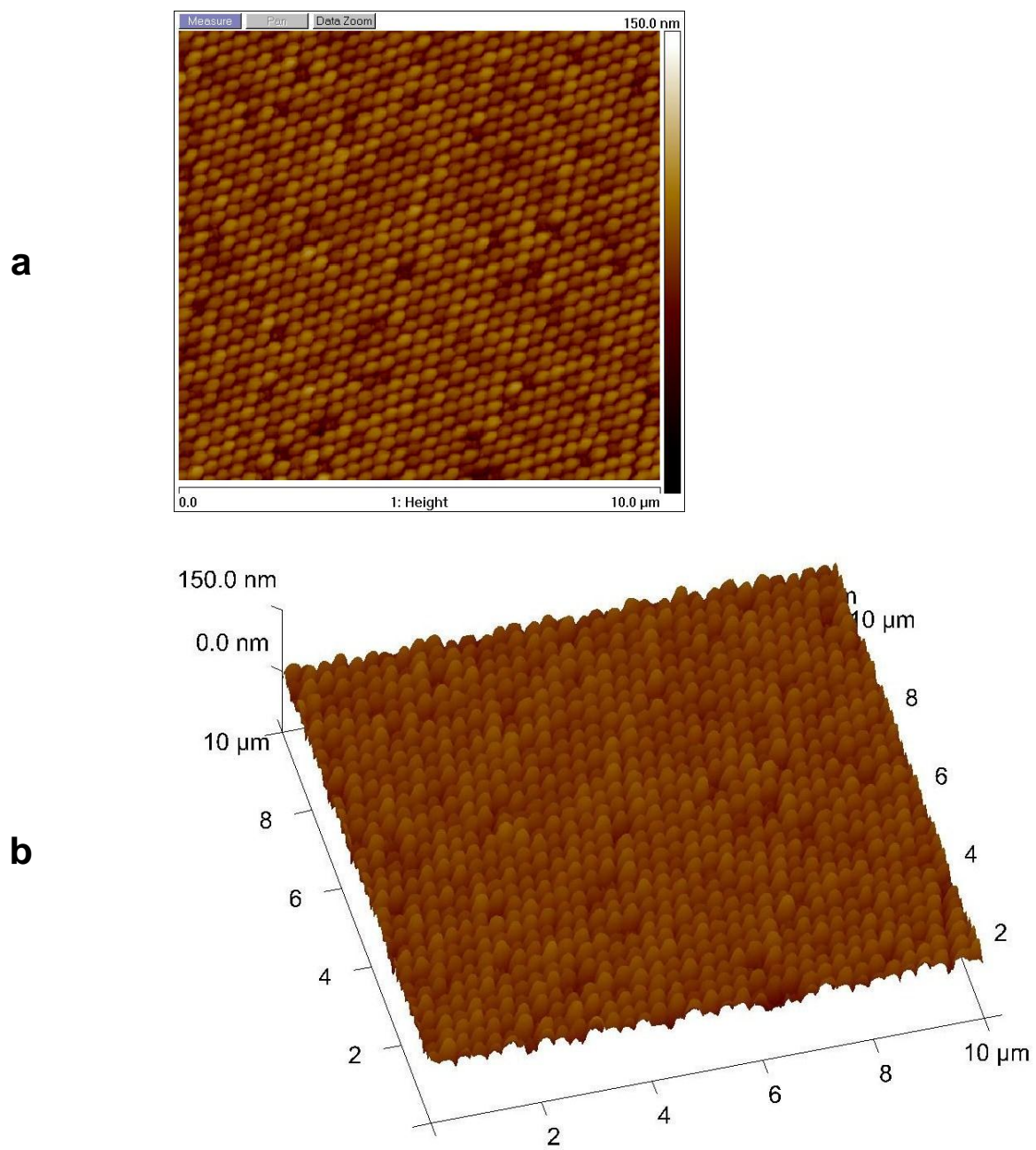


**Figure 2.9** Atomic force microscope topography image of the desiccator dried FON substrates as viewed from (a) above and (b) at an angle.

showed some HCP, but there were also many dislocations in the sphere monolayer, whereas the desiccator dried substrates showed much more uniform packing. Figures 2.10 & 2.11 show the SERS surface after ambient drying and desiccator drying, respectively.

### **2.3.5 SERS Substrate Stability**

The results from the first SERS substrates showed that the substrates in fact did enhance the Raman signal of the  $\text{LiFePO}_4$  enough to see the weaker anti-symmetric ( $\nu_3$ ) stretching bands at 1000 and 1070  $\text{cm}^{-1}$ . Unfortunately, the substrates were only viable for approximately one week, before the Raman spectra became irreproducible. “Ghost peaks” started appearing and the expected spectra of a strong symmetric band (950  $\text{cm}^{-1}$ ) and weaker anti-symmetric bands (1000 and 1070  $\text{cm}^{-1}$ ) transformed into a strong band at 1000  $\text{cm}^{-1}$  and weaker bands at 950 and 1070  $\text{cm}^{-1}$ . Spectra from the initial SERS experiments can be seen in Figure 2.12. This substrate degradation can be attributed to the oxidation of the silver on the surface.

After it was determined that the silver was the cause of the reproducibility issues, the decision was made to incorporate a bimetallic substrate in place of the Ag only substrate. The previous substrate preparation was modified to include Au as a protective top layer, because it resists oxidation and would therefore improve Raman signal reproducibility. The new substrate was prepared to have a base Ag layer of 140 nm and a top Au layer of 20 nm.

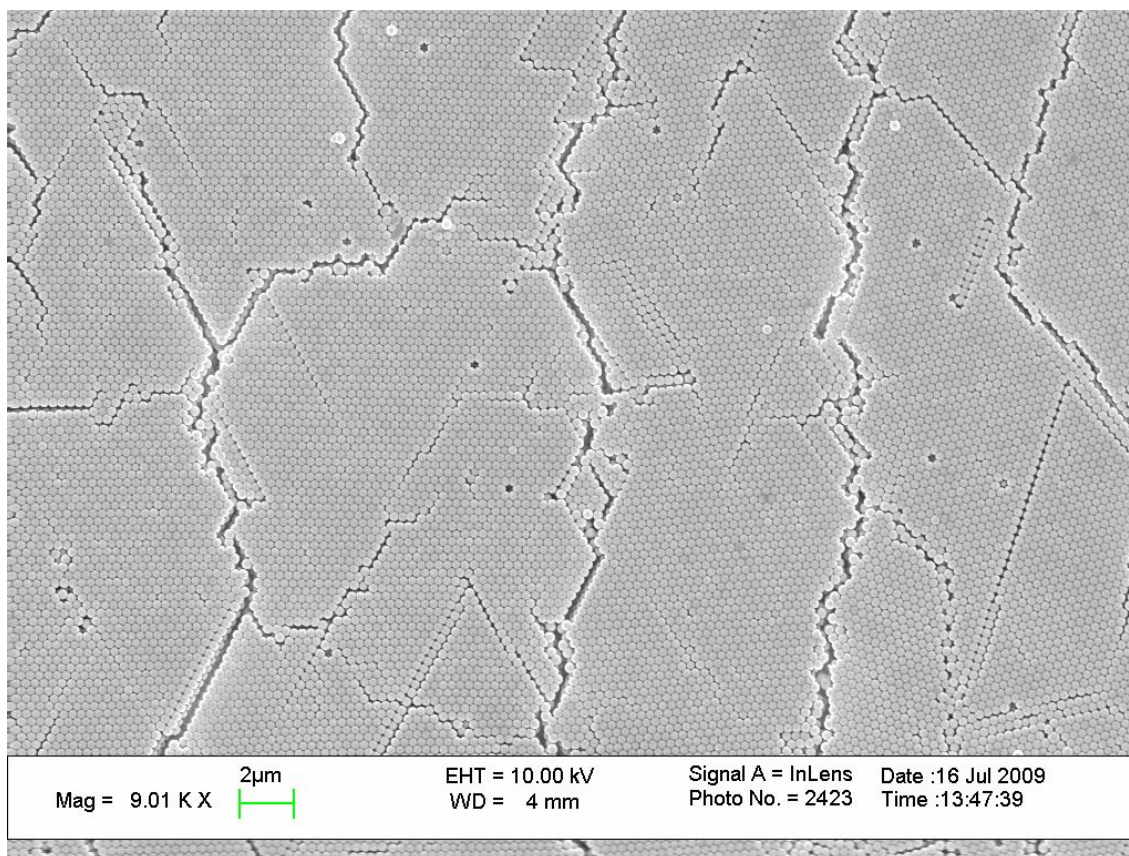


**Figure 2.10** SEM image of SERS substrate dried under ambient lab conditions.

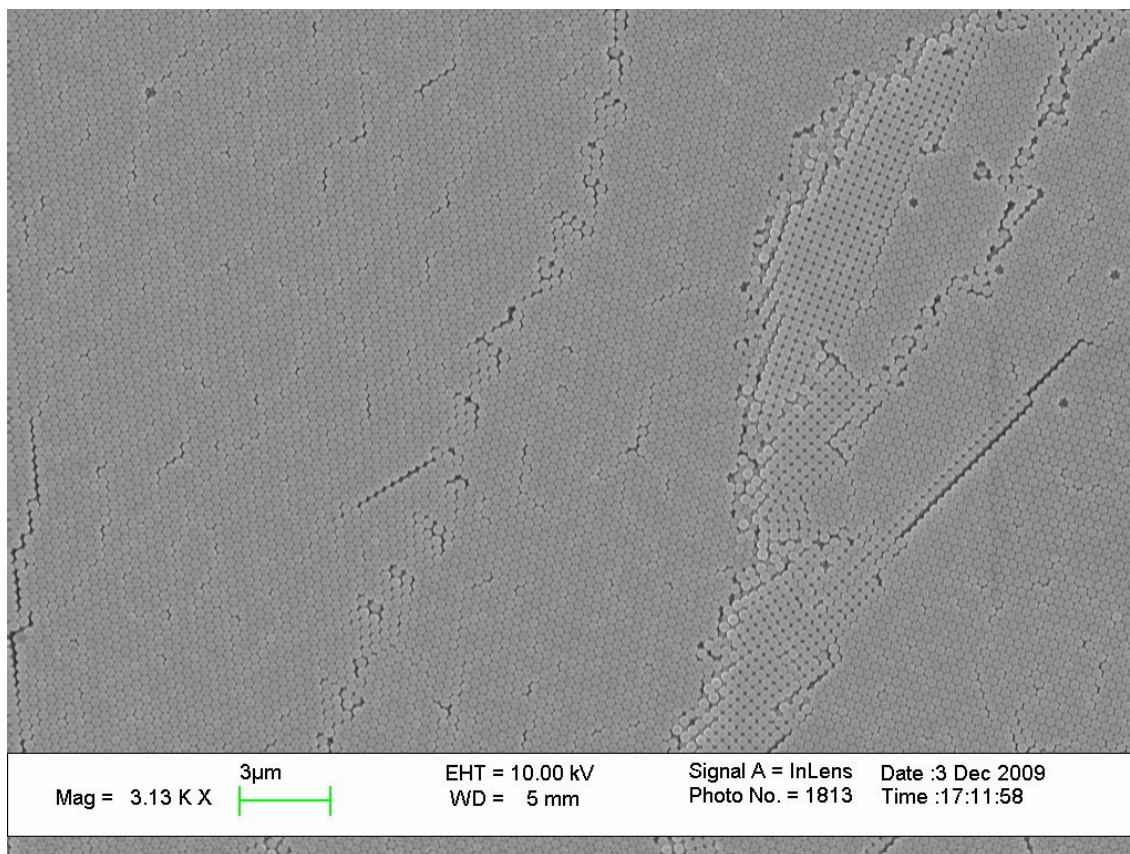


**Figure 2.11** SEM image of SERS substrate dried under desiccator drying conditions.

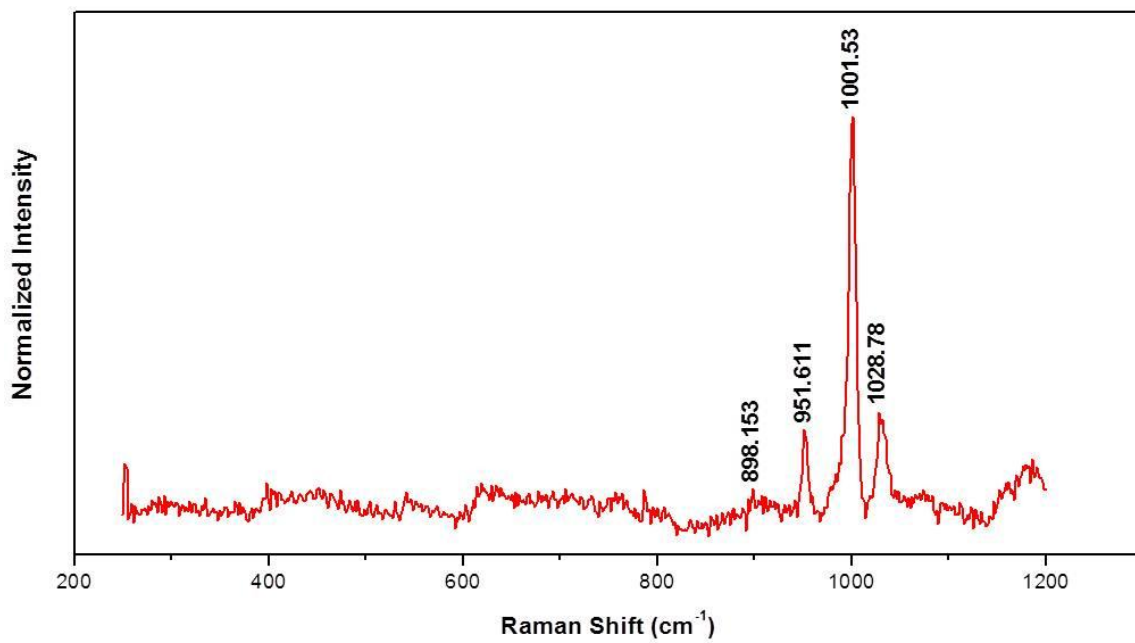


**Figure 2.12** LiFePO<sub>4</sub> Raman spectra from initial AgFON SERS substrates.

The  $\text{LiFePO}_4$  nanoparticles were deposited on the SERS substrate as described previously and once again analyzed via Raman. The resultant spectra showed strong, noticeably improved spectra of the symmetric and anti-symmetric stretches  $\nu_1$  and  $\nu_3$ . The spectra also showed bands emerging from the background in the  $200\text{-}700\text{ cm}^{-1}$  range. This range is also important to study due to the phase change information it yields. Surface enhanced spectra of  $\text{LiFePO}_4$  on the bimetallic SERS substrate is shown in Figure 2.13. The new SERS substrate preparation method has proven to greatly enhance the Raman spectra over the Ag only substrate. The signal improvement of the bimetallic SERS substrate vs. traditional Raman is shown in Figure 2.14. Along with the greater enhancement, the substrate has a longer shelf life and will remain in stable and usable for up to one month.

## 2.4 CONCLUSIONS

To this date, the Raman studies performed on  $\text{LiFePO}_4$  have been done on a bulk scale.<sup>25, 44, 45</sup> These studies have reported results that do not take into account the single nanoparticle intricacies because they are ensemble measurements. In Maccario et al.<sup>25</sup>, the authors studied electrodes made up of 80 wt% of carbon coated  $\text{LiFePO}_4$ , 10 wt% Super P conductive carbon and 10 wt% polyvinylidene fluoride (PVDF) as a binder. The inclusion of carbon in the studies of  $\text{LiFePO}_4$  is the case in most studies, since  $\text{LiFePO}_4$  is limited by its low electron conductivity.<sup>46</sup> Since the  $\text{LiFePO}_4$  signal weakness problem that was

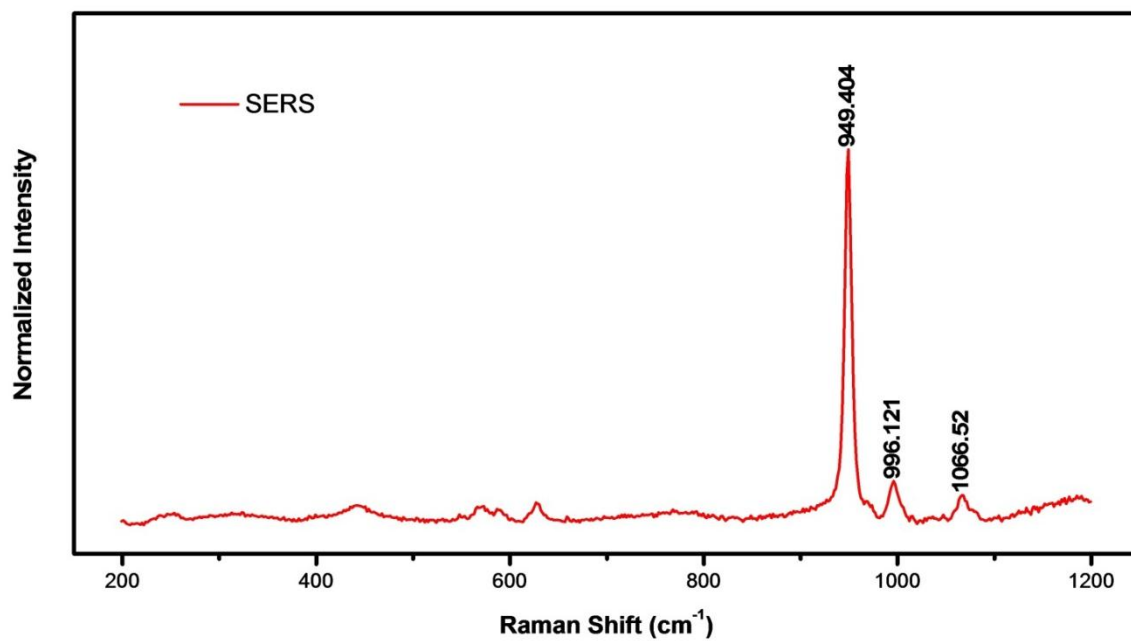


**Figure 2.13** Surface enhanced spectra of LiFePO<sub>4</sub> on the bimetallic SERS substrate.



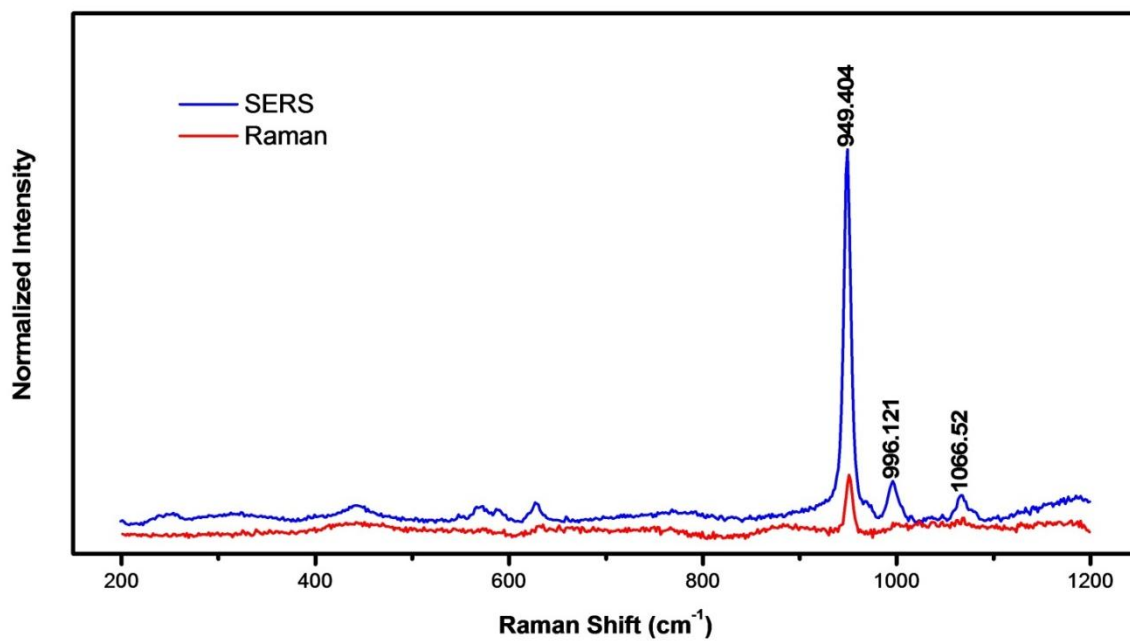


**Figure 2.14** LiFePO<sub>4</sub> comparison spectra of “traditional” Raman vs. SERS experiments.

encountered has been addressed by moving to SERS, the next step is to probe single nanoparticles on the SERS substrates. To accomplish this task, the nanoparticles need to be diluted to a value  $\leq 10^{-6}$  M to attain single nanoparticles on the surface of the SERS substrate. When this solution is deposited on the substrate and dried, the substrate can then be studied by SEM to confirm whether or not the nanoparticles are agglomerated or if they could be isolated on the surface. If the nanoparticles can be isolated, the resulting Raman spectra could shed light on the local and structural properties of the  $\text{LiFePO}_4$ .

## Chapter 3

### Electrochemical Cell Design

#### 3.1 INTRODUCTION

Now that the SERS substrate has been properly tuned for Raman studies, the  $\text{LiFePO}_4$ -coated substrate can be integrated into an electrochemical cell. The ultimate goal in this experiment is to study single  $\text{LiFePO}_4$  nanoparticles spectroelectrochemically to track phase changes while the cathode material is charged and discharged. Previous  $\text{LiFePO}_4$  studies have not focused on single nanoparticle electrochemical-SERS. Studies regarding SERS measurements in an electrochemical cell have been reported on molecular samples such as pyridine<sup>47</sup>, nitrobenzene<sup>48</sup> and thiocyanate<sup>49, 50</sup> to name a few.

There is an inherent challenge to integrating the SERS substrate into an electrochemical cell. The cell must be big enough to accommodate the substrate, while still being small enough to reduce the effect of IR drop. Our group has designed a cell that can integrate the SERS substrates coated with  $\text{LiFePO}_4$  nanoparticles. With this cell, surface enhanced Raman spectra of  $\text{LiFePO}_4$  can be collected simultaneously with electrochemical testing. This has not been previously reported. As previously discussed in Chapter 2, Burba et al.<sup>26</sup> showed ex-situ Raman results of various states of  $\text{LiFePO}_4$  lithiation. With the integration of the SERS substrate into the electrochemical cell, the ability to study in-situ surface enhanced Raman of  $\text{LiFePO}_4$  is possible. Studying  $\text{LiFePO}_4$  in-situ is important because the process by which lithium intercalates and de-intercalates

into the  $\text{FePO}_4$  olivine structure is not well understood. The lithiation and delithiation of  $\text{LiFePO}_4$  is proposed to proceed by a two phase process. In this process, the fully charged material is  $\text{FePO}_4$ , then goes to a two phase composition of  $\text{FePO}_4$  and  $\text{LiFePO}_4$  when partially charged and then returns to a single phase of  $\text{LiFePO}_4$  when fully discharged. In this process, there is an  $\text{LiFePO}_4/\text{FePO}_4$  interface as the nanoparticle is lithiated/delithiated.<sup>14</sup> Srinivasan et al.<sup>51</sup>, report a model that accounts for the phase change in  $\text{LiFePO}_4$ , showing that if the size of the  $\text{LiFePO}_4$  nanoparticle is small enough, the two-phase lithiation/delithiation process would change to a one-phase process. Gibot et al.<sup>52</sup> also showed that the two phase process can be forced to the one phase process by reducing the nanoparticle size. The  $\text{LiFePO}_4$  nanoparticle size was reduced to 50 nm from 100 nm in this study by Gibot and coworkers. Their study was a bulk electrode study, not a single nanoparticle study. Single nanoparticle studies would not average information like it is in XRD which is an ensemble technique. The ensemble study of bulk electrodes becomes a problem when explaining the complex processes, because it cannot precisely describe what is taking place in the single nanoparticles that make up the electrode.

## 3.2 EXPERIMENTAL

### 3.2.1 *in situ* SERS Electrochemical Cell Design

The electrochemical cell used in this study is made up of a glass cell with a volume of 10 ml, an aluminum 'eyepiece' with a quartz optical imaging window and an end cap containing plugs for counter and reference electrodes. Figure 3.1, shows a diagram of the electrochemical cell developed by our group. The reference and counter electrodes used are lithium foil. The electrolyte used is 1M Lithium Hexafluorophosphate ( $\text{LiPF}_6$ ) in 1:1 dimethyl carbonate/ethylene carbonate. The SERS substrate was cut into a 1 cm by 1 cm square to fit into the electrochemical cell. The substrate was mounted on a Teflon stage and electrical contact was made with titanium mesh. The working electrode is then screwed into the cell and the electrolyte is added. The end cap containing the reference and counter electrodes is then inserted, which completes the circuit. The fully assembled electrochemical cell is pictured from the top and side in Figure 3.2. The cell can be positioned under the Raman microscope and secured to prevent any vibrations that might be present from affecting the measurements. The charging and discharging of the cell is controlled by a CHI 660D potentiostat with three leads for the working, reference and counter electrode.

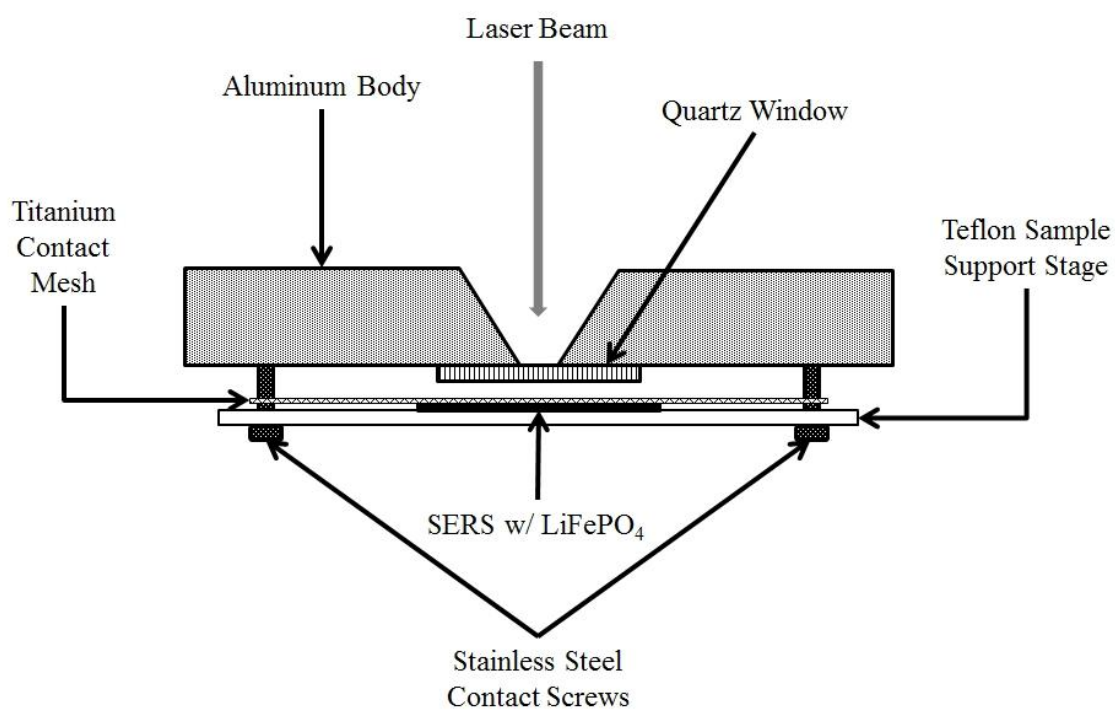


**Figure 3.1** A schematic of the working electrode of the electrochemical cell.

**a**



**b**



**Figure 3.2** (a) Top view and (b) side view of the electrochemical cell.

### **3.3 DISCUSSION AND CONCLUSIONS**

In this chapter the design of our electrochemical cell along with the addition of the SERS substrate to the electrochemical cell was discussed. Previous studies have only focused on bulk electrode Raman experiments, which are ensemble measurements. Since the signal of a single nanoparticle is going to be much lower than the bulk measurements previously reported, in-situ SERS is an ideal technique for this study. The incorporation of the SERS substrate into our electrochemical cell can allow for in situ Raman experiments to be carried out on a single nanoparticle scale.



## Chapter 4

### Isolation of LiFePO<sub>4</sub> Nanoparticles

#### 4.1 INTRODUCTION

The use of SERS has dramatically since it was introduced in 1977 as a means to detect single molecules.<sup>53</sup> Since then, SERS applications have been expanded to the study of nanoparticles, biological systems such as cancer detection. Composite organic-inorganic nanoparticles (COINs) are used under *in vivo* conditions in live animals such as mice.

As mentioned previously in Chapter 2, SEM is a powerful tool that is used to characterize nanomaterials. In this study it is used to investigate the prepared SERS substrates and can provide information supplemental to AFM. After analyzing the metal film over nanosphere (FON) substrate with AFM, the same substrate can be studied in the SEM chamber without any additional sample preparation. When the sample is analyzed in the chamber, with the electron beam accelerated to 10 kV, the surface can be imaged with a resolution comparable to that of AFM. Following the confirmation of isolated LiFePO<sub>4</sub> nanoparticles by SEM, the sample can be analyzed under the Raman microscope.

Another technique for studying non-bulk LiFePO<sub>4</sub> is using thin films. In Song et al.<sup>54</sup>, the authors used pulsed laser deposition to deposit thin films of LiFePO<sub>4</sub> onto stainless steel substrates. The Raman spectra of these thin films only showed the symmetric PO<sub>4</sub><sup>3-</sup> stretching band ~950 cm<sup>-1</sup>. The Raman spectra

of the isolated LiFePO<sub>4</sub> nanoparticle on the SERS substrates will be compared to the thin film study Raman results.

## **4.2 EXPERIMENTAL**

### **4.2.1 Single LiFePO<sub>4</sub> Nanoparticle Deposition**

Single LiFePO<sub>4</sub> nanoparticles are deposited onto the monolayer FON substrate. To achieve a uniform substrate coating of LiFePO<sub>4</sub>, a solution of the nanoparticles was made in ethanol. This solution was hand shaken and sonicated to evenly disperse the nanoparticles throughout the mixture. The first LiFePO<sub>4</sub> solution was prepared at a concentration of 10<sup>-3</sup> M.

## **4.3 RESULTS AND DISCUSSION**

### **4.3.1 Scanning Electron Microscopy**

Analysis by SEM showed this concentration of nanoparticles to be too high, with a large percentage of the surface covered and very little of the substrate surface visible. This presents a problem in the fact that, in order to fully utilize the enhancement of the metallic surface, the surface needs to be accessible to the excitation source. Figure 4.1 shows the substrate almost entirely covered by LiFePO<sub>4</sub> nanoparticles. The nanoparticle solution was further diluted to 10<sup>-6</sup> M to reduce the nanoparticle coverage on the substrate surface. The diluted LiFePO<sub>4</sub> solution was promptly drop cast, dried and imaged in the SEM. The reduction in nanoparticle concentration on the surface was confirmed by SEM and was an important step in the goal to achieve single nanoparticle

deposition. In Figure 4.2, agglomerated  $\text{LiFePO}_4$  nanoparticles can be seen on the SERS substrate. This figure confirms that the method is approaching where single nanoparticles can be deposited and studied by Raman, however further sample processing is necessary.

To accomplish this task, a small aliquot (1 mL) of the diluted  $\text{LiFePO}_4$  solution ( $10^{-6}$  M) was removed from the stock vial, placed in a small (1 dram) vial and sonicated for 60 minutes. The solution was deposited on the substrate surface and the ethanol was evaporated off in a vacuum oven. The sample was then analyzed by SEM to determine if the dilution was enough to produce single nanoparticles on the substrate surface. Now that single nanoparticle isolation on the SERS substrate has been confirmed by SEM, Raman studies can be conducted on the  $\text{LiFePO}_4$  nanoparticles. The next step of imaging a single  $\text{LiFePO}_4$  nanoparticle is a difficult task to undertake. The spot size of the excitation source is 2  $\mu\text{m}$ , whereas the size of the nanoparticles is  $<1$   $\mu\text{m}$  in length. It has proven to be difficult to locate single nanoparticles on the substrate surface due to the magnification and working distance of the objective.

#### **4.3.2 Raman Spectroscopy Studies**

The Renishaw Raman microscope was used with a 514.5 nm Argon ion laser excitation source, with the power output reduced to 5 mW and a 50X, N PLAN Leica objective, with a working distance of 0.37 mm is used to focus the laser on the substrate surface. After the initial testing of  $\text{LiFePO}_4$  nanoparticles on the SERS substrate surface confirmed that it was indeed possible to enhance

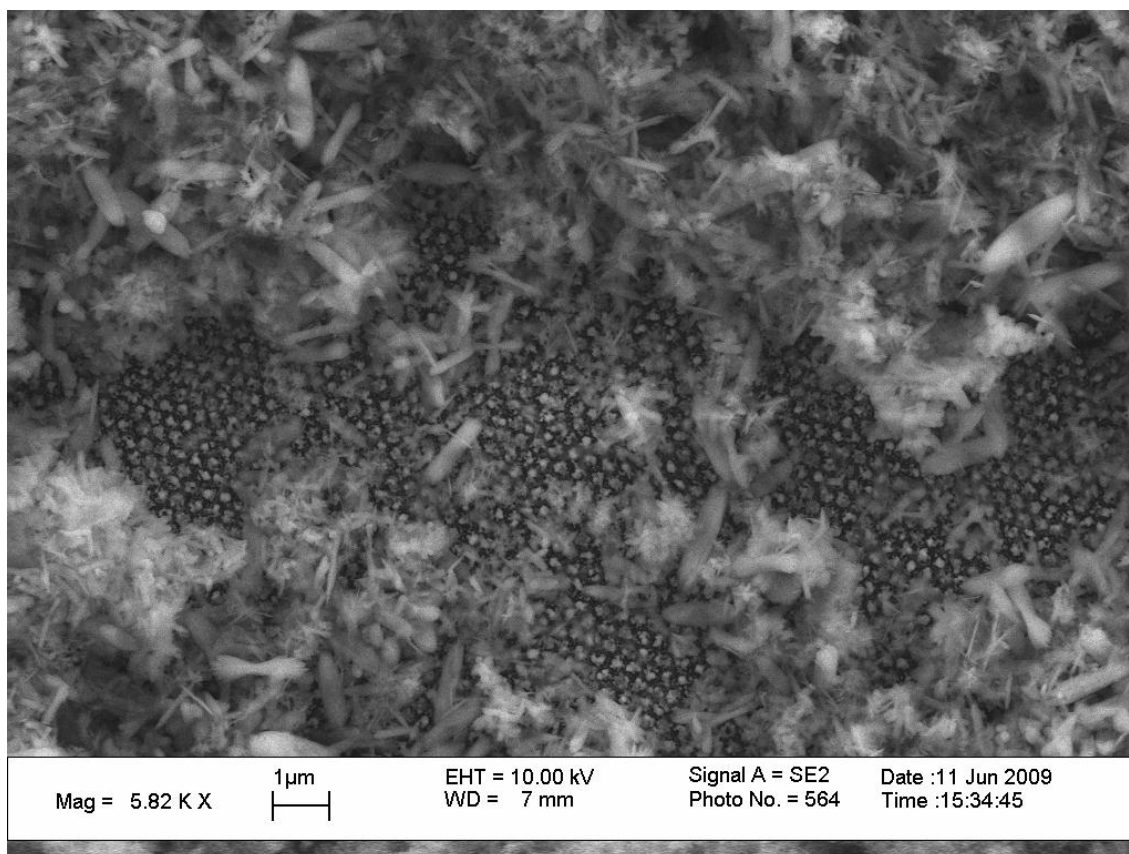


**Figure 4.1** SEM image of the SERS substrate covered with a high concentration of  $\text{LiFePO}_4$  nanoparticles.

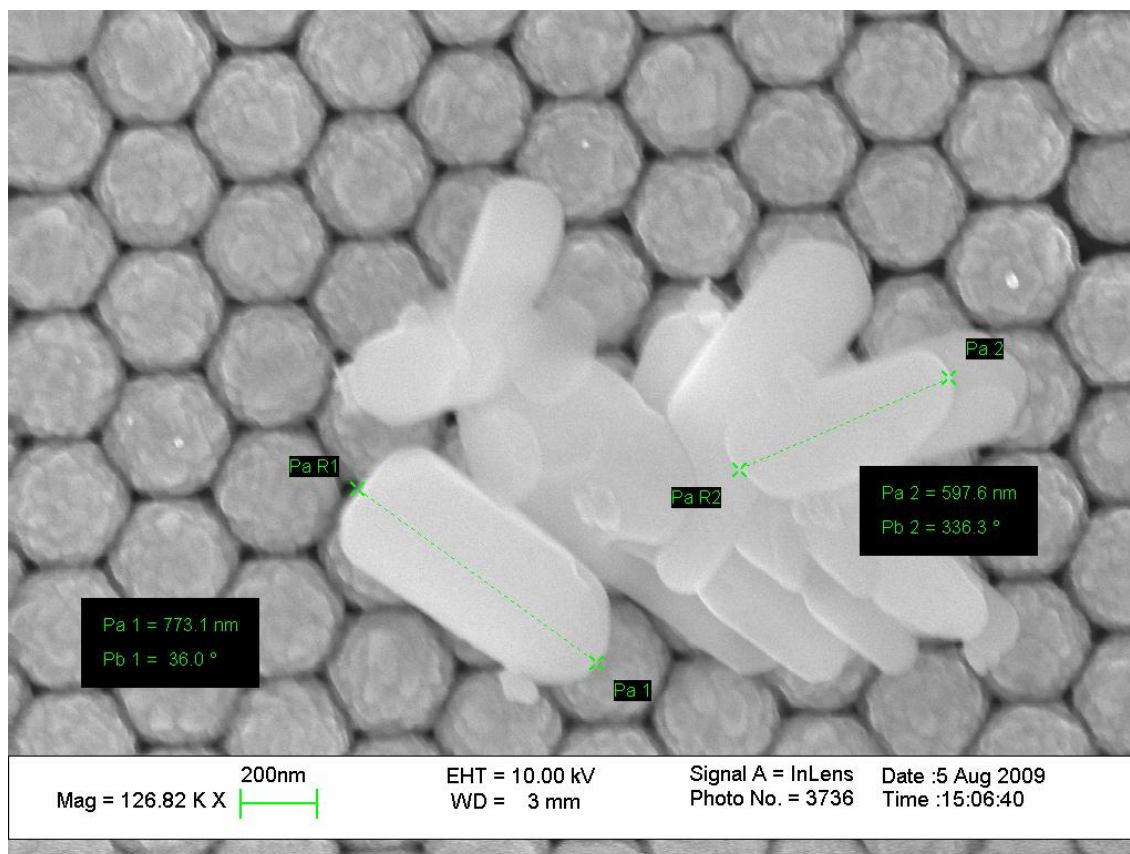


**Figure 4.2** SEM image of  $\text{LiFePO}_4$  nanoparticles isolated on the SERS substrate.

the signal, more detailed experiments followed. Raman experiments with the diluted nanoparticles ( $10^{-6}$  M) were done on the bimetallic Ag/Au SERS substrates. The symmetric ( $\sim 950\text{ cm}^{-1}$ ) and anti-symmetric ( $\sim 1000$  and  $\sim 1070\text{ cm}^{-1}$ )  $\text{PO}_4^{3-}$  stretching bands are characteristic to  $\text{LiFePO}_4$ . These bands were observed in the diluted  $\text{LiFePO}_4$  SERS samples. Figure 4.3 shows the Raman signal of isolated  $\text{LiFePO}_4$  nanoparticles.

#### **4.4 CONCLUSIONS**

The SERS spectra of the isolated  $\text{LiFePO}_4$  nanoparticles showed the three stretching bands of  $\text{PO}_4^{3-}$ , while the thin films studies reported by Song only detected the symmetric stretching band. This shows that SERS is a powerful tool for  $\text{LiFePO}_4$  nanoparticle studies. The use of SERS for Raman studies has greatly improved the Raman signal of the  $\text{LiFePO}_4$ . The process of preparing the SERS substrates, ensuring they dry and pack uniformly and also the use of the both Au and Ag have all contributed to this enhancement.

If another excitation source were to be used, simple adjustments can be made in the preparation process to tune the plasmon to between the excitation source and the scattered radiation from the  $\text{LiFePO}_4$ . Achieving single nanoparticles on the SERS substrate can be achieved as well. This lends to the notion that in-situ studies can follow the lithiation and delithiation of single  $\text{LiFePO}_4$  nanoparticles, which has not been reported previously.

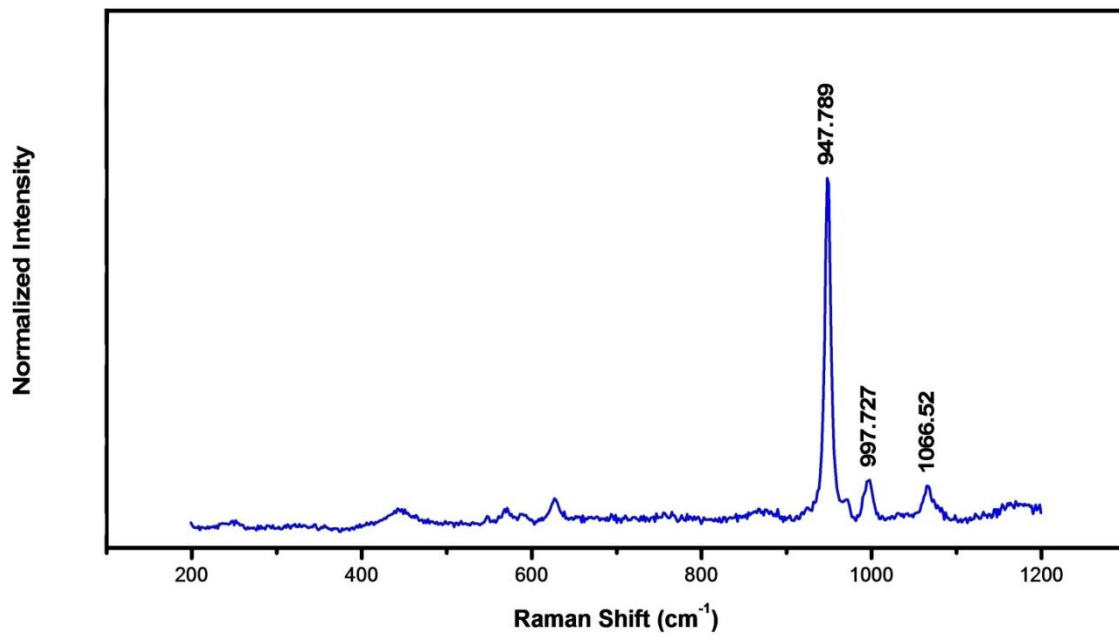


**Figure 4.3** SERS spectra of isolated LiFePO<sub>4</sub> nanoparticles.

## Chapter 5

### Future Directions

#### 5.1 INTRODUCTION

SERS has been demonstrated to be a successful tool for the enhancement  $\text{LiFePO}_4$  signal and can be applied to other energy storage materials. The advantage to this method is that instead of performing Raman experiments on bulk materials such as pressed pellets or coin cells, single nanocrystals/nanoparticles can be studied. The focus of most energy storage materials focus on the electrochemical properties of bulk materials. The fundamental understanding of how charge is transferred into and out of the individual nanoparticles that make up both anodes and cathodes in batteries is paramount in designing better batteries. The use of SERS to elicit and enhance spectra and structural information from  $\text{LiFePO}_4$  has been demonstrated in this work.

The analysis of  $\text{LiFePO}_4$  by the means of SERS is just a starting point. Furthermore, while the FON technique for  $\text{LiFePO}_4$  Raman studies has been proven successful for enhancing the Raman signal, there is room for improvement. Using metallic nanobowls as a substrate for SERS studies as described in Xu et al.<sup>55</sup> is a very appealing alternative to FON substrates. In that work, the authors described a way to prepare silver nanobowls via sphere lithography. In this system, the material of interest ( $\text{LiFePO}_4$ ) can be deposited in such a fashion that the nanoparticles would come to rest in the nanobowls similar



to eggs in an egg carton. With nanoparticle resting in this nanobowl, the nanoparticle interaction with the LSPR would be much greater than that of the nanoparticle simply resting on the surface of the FON substrate. SERS enhancement is distant dependent as described in Kennedy et al.<sup>56</sup>

Equation 5.1 – SERS Distance Dependence

$$I_{\text{SERS}} = \left( \frac{a + r}{a} \right)^{-10}$$

where  $a$  is the average size of the EM field enhancing features on the SERS surface and  $r$  is the distance between the sample and the surface. This equation indicates that the more contact that the sample has with the surface, the greater the signal will be enhanced.

In a preparation method attributed to the work done by Rybczynski et al.<sup>57</sup>, the authors created a monolayer of PS nanospheres on a silicon substrate by a self-assembly technique. This technique involved addition of PS spheres to a water surface in a beaker, the addition of a 2% docecylsodiumsulfate solution to order the pack the spheres on the surface and finally the removal of the ordered nanospheres with a clean silicon substrate. These ordered nanospheres are coated with 300 nm of silver and subsequently peeled off with normal sticking tape. The PS nanospheres were dissolved in a THF solution. This method was followed with the intent to employ the nanobowls as SERS substrates, with one

modification being that gold, instead of silver is used due to issues previously described.

## **5.2 EXPERIMENTAL**

### **5.2.1 Au Nanobowl Preparation**

Nanosphere lithography for the gold nanobowls was carried out according to Haynes et al.<sup>41</sup> and 150 nm of gold was deposited on the nanospheres after it was determined that if the film thickness was any greater, the tape was unable to peel off the gold. After the gold film was removed from the microscope cover slip, the tape was placed in a THF solution to dissolve the polystyrene spheres. As THF unfortunately caused the tape to curl up, preventing analysis and confirmation of the nanobowls via AFM, an alternative method of removing the PS spheres by using toluene was employed. The nanobowls were soaked in the toluene for 60 minutes to ensure complete PS dissolving, followed by rinsing with fresh toluene and drying under a stream of N<sub>2</sub> gas.

SEM is another analytical tool to characterize the gold nanobowls. There was a concern about whether or not the sticking tape would hold up to the electron beam. To remove any uncertainty of the tape possibly deforming while under analysis, carbon tape discs were employed to remove and support the nanobowls. The SERS substrates were prepared with the same nanosphere lithography method as before and the same amount of gold was deposited on the nanospheres. The use of the double sided carbon adhesive discs made SEM analysis easier, since it can be directly applied the pin stub sample mount. The

use of the double sided carbon adhesive discs also proved to be challenging, since it is not as rigid as sticking tape. It is likely to be stretched out and does not hold its disc shape if it is not handled carefully. To remove the gold films, the carbon disc is carefully placed on the edge of the SERS substrate. Approximately 90% of the disc should cover the substrate. This is to allow for easier peeling/removal of the gold film. The disc is then carefully removed from the substrate surface and placed on the pin stub sample mount. The sample mount containing the gold nanobowls/carbon disc is then placed in a beaker of toluene for 60 minutes to dissolve the PS. This time was determined to be optimal after analysis of 30, 45, 60 and 90 minute soaking times. The shorter times were not sufficient enough to completely remove the PS and the 90 minute soak completely removed the PS, but led to excessive disc swelling, which disturbed the uniformity of the nanobowls. After the sample was done soaking, it was dried under a stream of  $N_2$  gas. SEM analysis of the samples showed that the gold nanobowls were PS free however they were not completely uniform. This can be attributed to peeling the gold film off of the microscope cover slip and the swelling of the carbon disc.  $LiFePO_4$  can then be studied by Raman to see if it is comparable or offers signal enhancement improvements compared to FON substrates.

## **5.3 RESULTS AND DISCUSSION**

### **5.3.1 Atomic Force Microscopy**

AFM analysis confirmed that the surface was composed of uniform nanobowls and was free of any PS spheres. It was also used to confirm that the nanobowl size corresponded to the size (i.e. nanobowl diameter) of the nanospheres used in the nanosphere lithography. In Figure 5.1, the uniformity and periodicity can be seen of the Au nanobowls is shown. Figure 5.2, confirms that that the substrate preparation produced highly uniform nanobowls and shows the unique geometry of the nanobowl. The raised edges of these nanobowls are the regions in which the highest EM enhancement takes place.

### **5.3.2 Scanning Electron Microscopy**

Analysis of the SERS substrates with SEM was again beneficial due to the conducting nature of the substrates. The information obtained was complementary to the AFM data and allowed for wider images of the nanobowl substrates to determine long range order. Figure 5.3 shows the order of the Au nanobowl after removing them from the FON substrates with adhesive tape. SEM allowed for imaging of the  $\text{LiFePO}_4$  nanoparticles in the nanobowls. Figure 5.4 shows  $\text{LiFePO}_4$  nanoparticles in the Au nanobowls. This information will aid in making smaller nanobowl so more of the nanoparticle surface area will be in contact of the nanobowl to generate greater Raman signal.

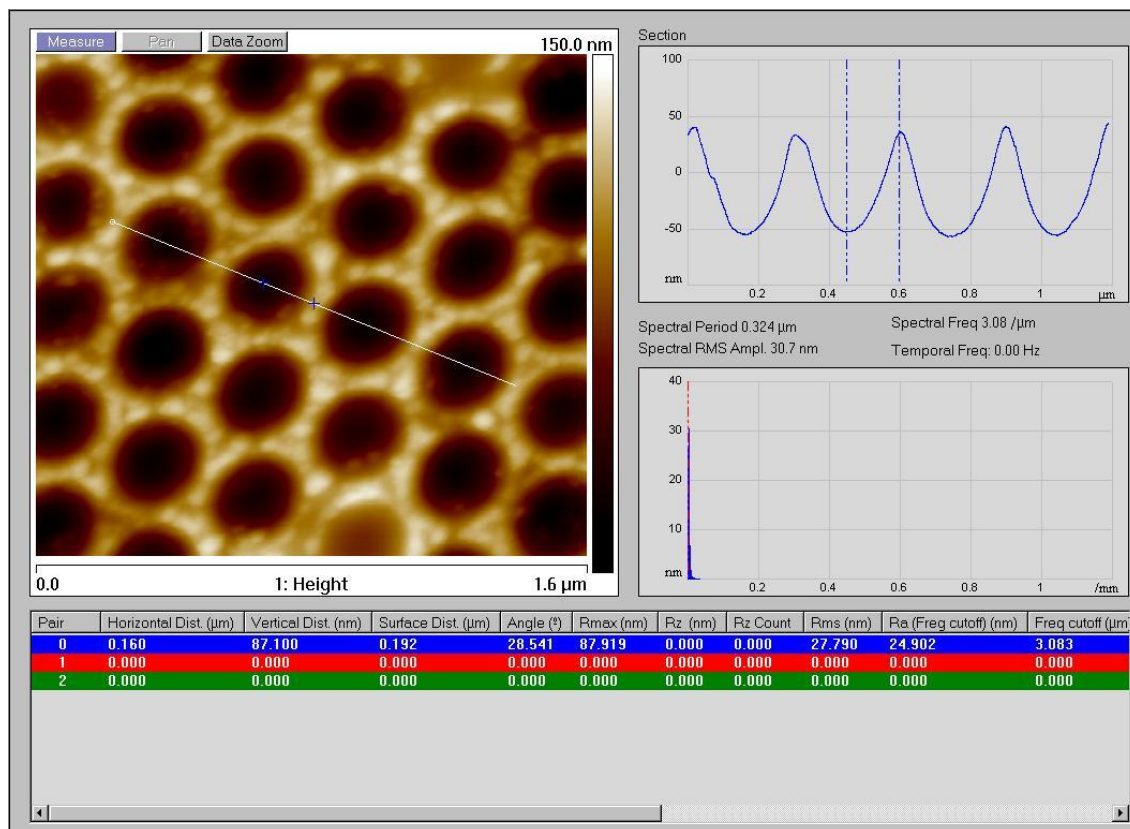


**Figure 5.1** Atomic force microscope image of Au nanobowl, with surface periodicity on right.

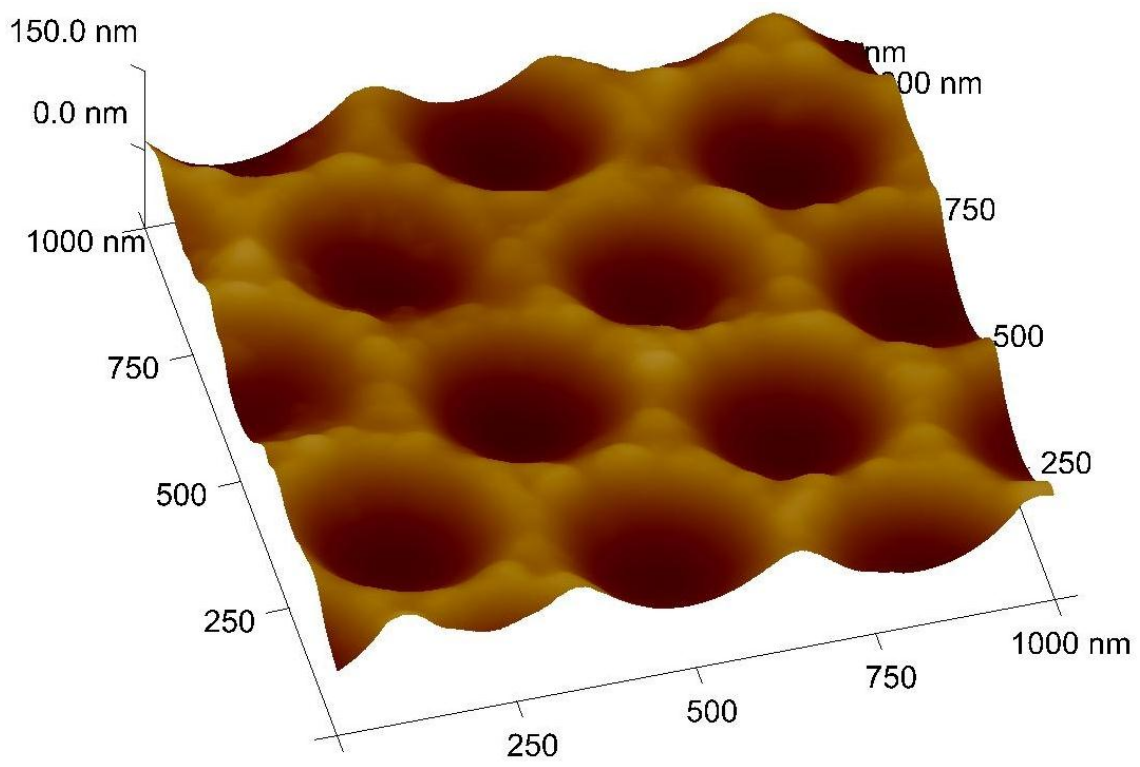


**Figure 5.2** Atomic force microscope topography image of Au nanobowls at an angle.

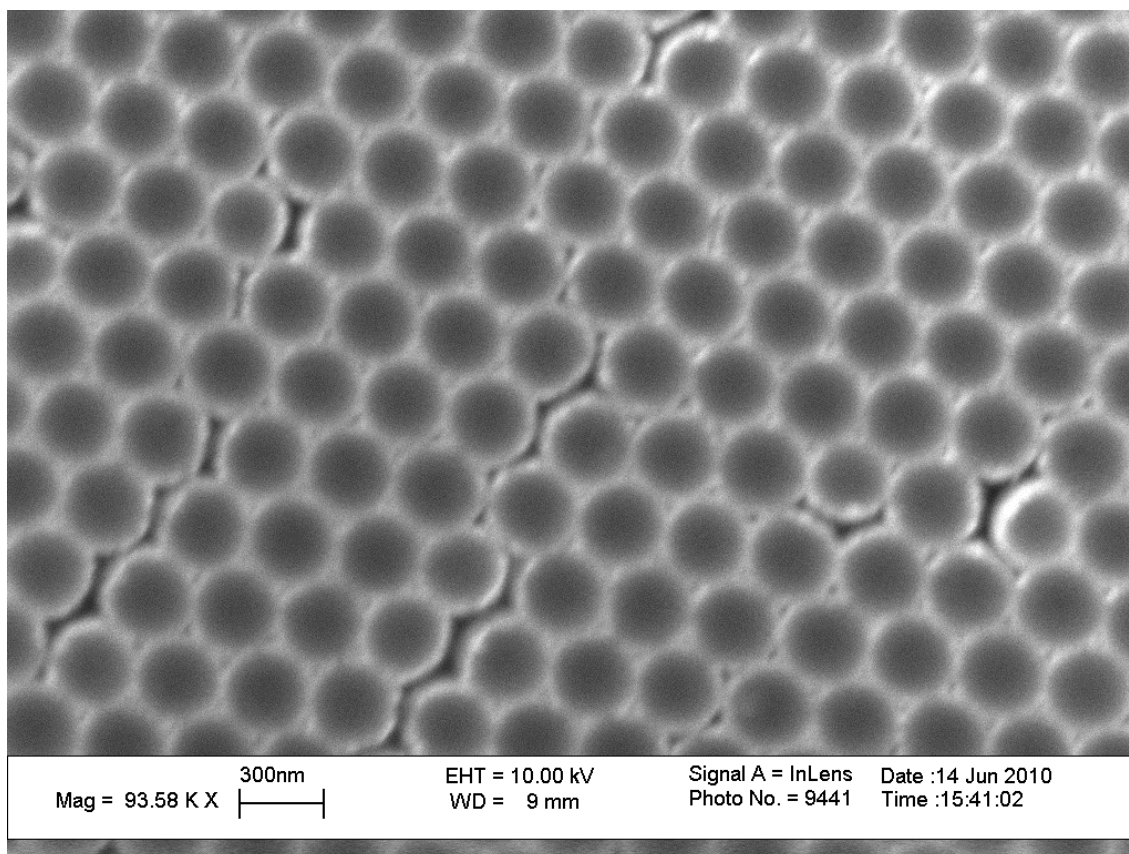


**Figure 5.3** SEM image of highly ordered Au nanobowls.

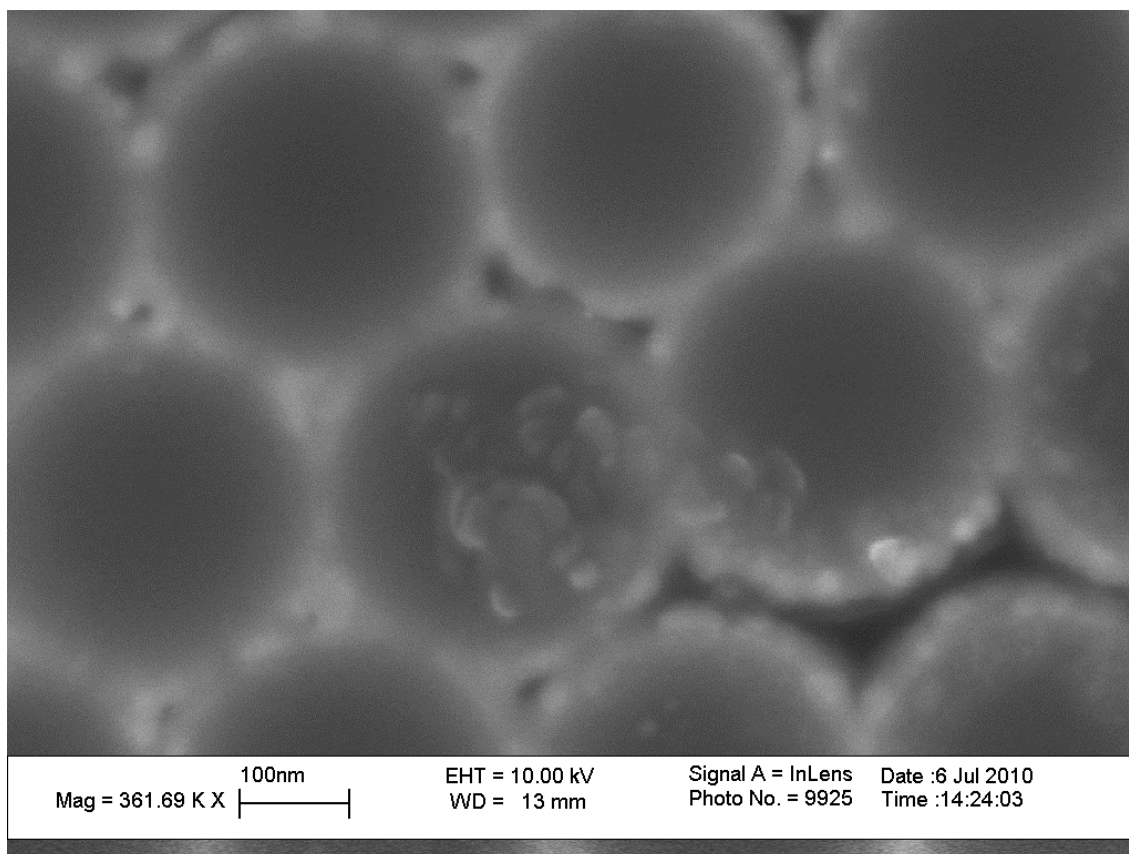


**Figure 5.4** SEM image of  $\text{LiFePO}_4$  nanoparticle deposited in Au nanobowls.



## 5.4 CONCLUSIONS

The results from the Raman studies can be used to optimize the nanobowl preparation method. Optimization of these nanobowls can proceed from two fronts: metal thickness variation and nanosphere diameter variation. Changing the thickness of the metal could yield better surface enhancement due to the increase in conducting electrons present. Changing the size of the nanobowls by changing the diameter of the nanosphere used could also lead to surface enhancement because the nanobowl could be custom tailored to the size of the nanoparticle of interest. Chen et al.<sup>58</sup> describes an alternative method of creating large scale nanobowls that would remove the need to use an adhesive surface to remove the metal film. In his work, the authors created metallic nanobowls by nanosphere lithography on silicon, followed by thermal deposition of a thin layer (50 nm) of gold. A thick layer (200  $\mu\text{m}$ ) of nickel is then electrochemically deposited on the gold layer using a nickel sulfamate solution. The PS nanospheres are removed by ultrasonication in ethanol, leaving the gold film with a rigid nickel support. This method would allow for SERS substrates with long range ordered nanobowls and the flexibility to tune the substrate to the desired parameters, as well as the capability of incorporation into an electrochemical cell without further modification. As energy storage materials evolve and improve, SERS will be a necessary tool to help explain the electrochemical processes taking place. Improvement of SERS substrates will also need to be made to keep pace with the technology and complexity of energy storage materials.

## References

1. United States Dept. of Energy, B. E. S. A. C. *Basic Research Needs for Electrical Energy Storage*; Office of Basic Energy Sciences, U.S. Department of Energy: Washington, D.C., 2007.
2. Petrova, D.; Dombalov, I., Influence Of Some Anthropogenic Factors On The Global Warming. *J. Environ. Prot. Ecol.* **2003**, 4, 894-899.
3. Stewart, S. G.; Srinivasan, V.; Newman, J., Modeling the performance of lithium-ion batteries and capacitors during hybrid-electric-vehicle operation. *J. Electrochem. Soc.* **2008**, 155, (9), A664-a671.
4. Whittingham, M. S., Materials challenges facing electrical energy storage. *MRS Bull.* **2008**, 33, (4), 411-419.
5. Tarascon, J. M.; Armand, M., Issues and challenges facing rechargeable lithium batteries. *Nature* **2001**, 414, (6861), 359-367.
6. Shao-Horn, Y.; Croguennec, L.; Delmas, C.; Nelson, E. C.; O'Keefe, M. A., Atomic resolution of lithium ions in LiCoO<sub>2</sub>. *Nat. Mater.* **2003**, 2, (7), 464-467.
7. Muraliganth, T.; Murugan, A. V.; Manthiram, A., Nanoscale networking of LiFePO<sub>4</sub> nanorods synthesized by a microwave-solvothermal route with carbon nanotubes for lithium ion batteries. *J. Mater. Chem.* **2008**, 18, (46), 5661-5668.
8. Schwartz, M. M., *Smart Materials*. CRC Press: Boca Raton, 2008.
9. Amatucci, G. G.; Tarascon, J. M.; Klein, L. C., CoO<sub>2</sub>, The End Member of the Li<sub>x</sub>CoO<sub>2</sub> Solid Solution. *J. Electrochem. Soc.* **1996**, 143, (3), 1114-1123.
10. Tateishi, K.; Suda, K.; du Boulay, D.; Ishizawa, N.; Oishi, S., LiMn<sub>2</sub>O<sub>4</sub>: a spinel-related low-temperature modification. *Acta Crystallogr. E* **2004**, 60, I18-I21.

11. Ellis, B. L.; Lee, K. T.; Nazar, L. F., Positive Electrode Materials for Li-Ion and Li-Batteries. *Chem. Mater.* **2010**, *22*, (3), 691-714.
12. Delacourt, C.; Poizot, P.; Levasseur, S.; Masquelier, C., Size effects on carbon-free LiFePO<sub>4</sub> powders. *Electrochemical and Solid State Letters* **2006**, *9*, (7), A352-a355.
13. Delmas, C.; Maccario, M.; Croguennec, L.; Le Cras, F.; Weill, F., Lithium deintercalation in LiFePO<sub>4</sub> nanoparticles via a domino-cascade model. *Nature Materials* **2008**, *7*, (8), 665-671.
14. Padhi, A. K.; Nanjundaswamy, K. S.; Goodenough, J. B., Phospho-olivines as positive-electrode materials for rechargeable lithium batteries. *J. Electrochem. Soc.* **1997**, *144*, (4), 1188-1194.
15. Goodenough, J.; Kim, Y., Challenges for Rechargeable Li Batteries. *Chem. Mater.* **2010**, *22*, (3), 587-603.
16. Tang, P.; Holzwarth, N. A. W., Electronic structure of FePO<sub>4</sub>, LiFePO<sub>4</sub>, and related materials. *Phys. Rev. B* **2003**, *68*, (16), 165107.
17. Balbuena, P. B.; Wang, Y., *Lithium-Ion Batteries*. Imperial College Press: London, 2004.
18. Peled, E., The Electrochemical-Behavior of Alkali and Alkaline-Earth Metals in Non-Aqueous Battery Systems - the Solid Electrolyte Interphase Model. *J. Electrochem. Soc.* **1979**, *126*, (12), 2047-2051.
19. Peled, E.; Golodnitsky, D.; Ardel, G.; Menachem, C.; Tow, D. B.; Eshkenazy, V., The role of SEI in lithium and lithium ion batteries. *Mater. Res. Soc. Symp. P* **1995**, *393*, 209-221.
20. Ramana, C. V.; Mauger, A.; Gendron, F.; Julien, C. M.; Zaghbi, K., Study of the Li-insertion/extraction process in LiFePO<sub>4</sub>/FePO<sub>4</sub>. *J. Power Sources* **2009**, *187*, (2), 555-564.
21. Kobayashi, G.; Nishimura, S. I.; Park, M. S.; Kanno, R.; Yashima, M.; Ida, T.; Yamada, A., Isolation of Solid Solution Phases in Size-Controlled Li<sub>x</sub>FePO<sub>4</sub> at Room Temperature. *Adv. Funct. Mater.* **2009**, *19*, (3), 395-403.

22. Murugan, A.; Muraliganth, T.; Manthiram, A., One-Pot Microwave-Hydrothermal Synthesis and Characterization of Carbon-Coated  $\text{LiMPO}_4$  (M = Mn, Fe, and Co) Cathodes. *J. Electrochem. Soc.* **2009**, 156, (2), A79-A83.
23. Murugan, A. V.; Muraliganth, T.; Ferreira, P. J.; Manthiram, A., Dimensionally Modulated, Single-Crystalline  $\text{LiMPO}_4$  (M = Mn, Fe, Co, and Ni) with Nano-Thumblike Shapes for High-Power Energy Storage. *Inorg. Chem.* **2009**, 48, (3), 946-952.
24. Yamada, A.; Nishimura, S.; Koizumi, H.; Kanno, R.; Seki, S.; Kobayashi, Y.; Miyashiro, H.; Dodd, J.; Yazami, R.; Fultz, B., Intermediate phases in  $\text{Li}_x\text{FePO}_4$ . *Mater. Res. Soc. Symp. P* **2007**, 972, 257-264.
25. Maccario, M.; Croguennec, L.; Desbat, B.; Couzi, M.; Le Cras, F.; Servant, L., Raman and FTIR Spectroscopy Investigations of Carbon-Coated  $\text{Li}_x\text{FePO}_4$  Materials. *J. Electrochem. Soc.* **2008**, 155, (12), A879-a886.
26. Burba, C. M.; Frech, R., Raman and FTIR spectroscopic study of  $\text{Li}_x\text{FePO}_4$  ( $0 < x < 1$ ). *J. Electrochem. Soc.* **2004**, 151, (7), A1032-a1038.
27. Croce, F.; Epifanio, A. D.; Hassoun, J.; Deptula, A.; Olczac, T.; Scrosati, B., A novel concept for the synthesis of an improved  $\text{LiFePO}_4$  lithium battery cathode. *Electrochem. Solid St.* **2002**, 5, (3), A47-A50.
28. Kim, D. H.; Kim, J., Synthesis of  $\text{LiFePO}_4$  nanoparticles in polyol medium and their electrochemical properties. *Electrochem. Solid St.* **2006**, 9, (9), A439-A442.
29. Murugan, A. V.; Muraliganth, T.; Manthiram, A., Comparison of microwave assisted solvothermal and hydrothermal syntheses of  $\text{LiFePO}_4/\text{C}$  nanocomposite cathodes for lithium ion batteries. *J. Phys. Chem. C* **2008**, 112, (37), 14665-14671.
30. Paraguassu, W.; Freire, P. T. C.; Lemos, V.; Lala, S. M.; Montoro, L. A.; Rosolen, J. M., Phonon calculation on olivine-like  $\text{LiMPO}_4$  (M = Ni, Co, Fe) and Raman scattering of the iron-containing compound. *J. Raman Spectrosc.* **2005**, 36, (3), 213-220.
31. Baddour-Hadjean, R.; Pereira-Ramos, J. P., Raman Microspectrometry Applied to the Study of Electrode Materials for Lithium Batteries. *Chem. Rev.* **2010**, 110, (3), 1278-1319.

32. Popovic, L.; de Waal, D.; Boeyens, J. C. A., Correlation between Raman wavenumbers and P-O bond lengths in crystalline inorganic phosphates. *Journal of Raman Spectroscopy* **2005**, 36, (1), 2-11.
33. Nakamoto, K., *Infrared and Raman Spectra of Inorganic and Coordination Compounds*. 6th ed.; Wiley: Hoboken, N.J., 2009; p v. <1->.
34. Stiles, P. L.; Dieringer, J. A.; Shah, N. C.; Van Duyne, R. R., Surface-Enhanced Raman Spectroscopy. *Ann. Rev. Anal. Chem.* **2008**, 1, 601-626.
35. Nie, S.; Emory, S. R., Probing Single Molecules and Single Nanoparticles by Surface-Enhanced Raman Scattering. *Science* **1997**, 275, (5303), 1102-1106.
36. Kneipp, K.; Wang, Y.; Kneipp, H.; Perelman, L. T.; Itzkan, I.; Dasari, R. R.; Feld, M. S., Single Molecule Detection Using Surface-Enhanced Raman Scattering (SERS). *Phys. Rev. Lett.* **1997**, 78, (9), 1667.
37. Willets, K. A.; Van Duyne, R. P., Localized Surface Plasmon Resonance Spectroscopy and Sensing. *Ann. Rev. Phys. Chem.* **2007**, 58, 267-297.
38. Dieringer, J. A.; Wustholz, K. L.; Masiello, D. J.; Camden, J. P.; Kleinman, S. L.; Schatz, G. C.; Van Duyne, R. P., Surface-Enhanced Raman Excitation Spectroscopy of a Single Rhodamine 6G Molecule. *J. Am. Chem. Soc.* **2009**, 131, (2), 849-854.
39. Schwartzberg, A. M.; Grant, C. D.; Wolcott, A.; Bogomolni, R.; Zhang, J. Z., Synthesis and characterization of gold nanoparticle aggregates as novel substrates for surface enhanced Raman scattering. *P. Soc. Photo-Opt. Ins.* **2003**, 5221, 100-107
40. Balmes, O.; Bovin, J. O.; Malm, J. O.; Xu, H. X., Homogeneous surface-enhanced Raman scattering observed from self-assembled gold nanoparticle films deposited from the liquid-liquid interface. *Vib. Spectrosc.* **2005**, 37, (2), 189-193.
41. Haynes, C. L.; Van Duyne, R. P., Nanosphere lithography: A versatile nanofabrication tool for studies of size-dependent nanoparticle optics. *J. Phys. Chem. B* **2001**, 105, (24), 5599-5611.

42. Van Duyne, R. P.; Hulteen, J. C.; Treichel, D. A., Atomic-Force Microscopy and Surface-Enhanced Raman-Spectroscopy.1. Ag Island Films and Ag Film over Polymer Nanosphere Surfaces Supported on Glass. *J. Chem. Phys.* **1993**, 99, (3), 2101-2115.
43. Van Duyne, R. P.; Hulteen, J. C.; Treichel, D. A., Atomic-Force Microscopy and Surface-Enhanced Raman-Spectroscopy.1. Ag Island Films and Ag Film over Polymer Nanosphere Surfaces Supported on Glass. *J. Chem. Phys.* **1993**, 99, (3), 2101-2115.
44. Ni, J. F.; Morishita, M.; Kawabe, Y.; Watada, M.; Takeichi, N.; Sakai, T., Hydrothermal preparation of LiFePO<sub>4</sub> nanocrystals mediated by organic acid. *J. Power Sources* **2010**, 195, (9), 2877-2882.
45. Rangappa, D.; Ichihara, M.; Kudo, T.; Honma, I., Surface modified LiFePO<sub>4</sub>/C nanocrystals synthesis by organic molecules assisted supercritical water process. *J. Power Sources* **2009**, 194, (2), 1036-1042.
46. Chung, S. Y.; Bloking, J. T.; Chiang, Y. M., Electronically conductive phospho-olivines as lithium storage electrodes. *Nat. Mater.* **2002**, 1, (2), 123-128.
47. Wu, D. Y.; Li, J. F.; Ren, B.; Tian, Z. Q., Electrochemical surface-enhanced Raman spectroscopy of nanostructures. *Chem. Soc. Rev.* **2008**, 37, (5), 1025-1041.
48. Gao, P.; Gosztola, D.; Weaver, M. J., Surface-enhanced raman spectroscopy as a probe of electroorganic reaction pathways. 1. Processes involving adsorbed nitrobenzene, azobenzene, and related species. *J. Phys. Chem.* **1988**, 92, (25), 7122.
49. Oklejas, V.; Harris, J. M., Potential-dependent surface-enhanced Raman scattering from adsorbed thiocyanate for characterizing silver surfaces with improved reproducibility. *Appl. Spectrosc.* **2004**, 58, (8), 945-951.
50. Weaver, M. J.; Barz, F.; Gordon li, J. G.; Philpott, M. R., Surface-enhanced Raman spectroscopy of electrochemically characterized interfaces; potential dependence of Raman spectra for thiocyanate at silver electrodes. *Surf. Sci.* **1983**, 125, (2), 409.
51. Srinivasan, V.; Newman, J., Discharge model for the lithium iron-phosphate electrode. *J. Electrochem. Soc.* **2004**, 151, (10), A1517-a1529.

52. Gibot, P.; Casas-Cabanas, M.; Laffont, L.; Levasseur, S.; Carlach, P.; Hamelet, S.; Tarascon, J. M.; Masquelier, C., Room-temperature single-phase Li insertion/extraction in nanoscale  $\text{Li}_x\text{FePO}_4$ . *Nat. Mater.* **2008**, *7*, (9), 741-747.
53. Jeanmaire, D. L.; Van Duyne, R. P., Surface Raman Spectroelectrochemistry. 1. Heterocyclic, Aromatic, and Aliphatic-Amines Adsorbed on Anodized Silver Electrode. *J. Electroanal. Chem.* **1977**, *84*, (1), 1-20.
54. Song, S. W.; Reade, R. P.; Kostecki, R.; Striebel, K. A., Electrochemical studies of the  $\text{LiFePO}_4$  thin films prepared with pulsed laser deposition. *J. Electrochem. Soc.* **2006**, *153*, (1), A12-a19.
55. Xu, M. J.; Lu, N.; Xu, H. B.; Qi, D. P.; Wang, Y. D.; Chi, L. F., Fabrication of Functional Silver Nanobowl Arrays via Sphere Lithography. *Langmuir* **2009**, *25*, (19), 11216-11220.
56. Kennedy, B. J.; Spaeth, S.; Dickey, M.; Carron, K. T., Determination of the distance dependence and experimental effects for modified SERS substrates based on self-assembled monolayers formed using alkanethiols. *J. Phys. Chem. B* **1999**, *103*, (18), 3640-3646.
57. Rybczynski, J.; Hilgendorff, M.; Giersig, M., Nanosphere Lithography - Fabrication of Various Periodic Magnetic Particle Arrays Using Versatile Nanosphere Masks. In *Low-Dimensional Systems: Theory, Preparation, and Some Applications*, Liz-Marzán, L. M.; Giersig, M., Eds. Kluwer Academic Publishers: Dordrecht; Boston, 2003; pp 163-172.
58. Chen, X.; Wei, X.; Jiang, K., Large-scale fabrication of ordered metallic hybrid nanostructures. *Opt. Express* **2008**, *16*, (16), 11888-11893.

## **Vita**

Nicholas Ryan Delone, the son of Herbert and Carolyn Delone, was born December 17, 1984 in Alamogordo, NM. After graduating from Alamogordo High School in 2003, he enrolled at Texas Tech University in Lubbock, TX. He graduated with a Bachelor of Science in Chemistry and Mathematics minor from Texas Tech in August 2007. He entered The University of Texas at Austin in August 2008 to begin his graduate studies under the guidance of Professor Keith J. Stevenson.

Permanent address: 733 Eagle Drive, Alamogordo, NM 88310

This thesis was typed by the author.